NACA RM E54J18

NACA

RESEARCH MEMORANDUM

ROTATING-STALL AND ROTOR-BLADE-VIBRATION SURVEY OF A 13-STAGE AXIAL-FLOW COMPRESSOR IN A TURBOJET ENGINE

By Howard F. Calvert, Willis M. Braithwaite, and Arthur A. Medeiros

Lewis Flight Propulsion Laboratory
Cleveland, Ohio

NATIONAL ADVISORY COMMITTEE FOR AERONAUTICS

WASHINGTON
April 29, 1955
Declassified March 18, 1960

NACA RM E54J18

NATIONAL ADVISORY COMMITTEE FOR AERONAUTICS

RESEARCH MEMORANDUM

ROTATING-STALL AND ROTOR-BLADE-VIBRATION SURVEY OF A 13-STAGE AXIAL-FLOW COMPRESSOR IN A TURBOJET ENGINE

By Howard F. Calvert, Willis M. Braithwaite, and Arthur A. Medeiros

SUMMARY

A blade-vibration and rotating-stall survey was conducted on a production turbojet engine incorporating a 13-stage axial-flow compressor with a pressure ratio of approximately 7 and an air flow of 120 pounds per second. Resistance-wire strain gages and constant-current hot-wire anemometers were used to measure the blade vibrations and rotating stall.

Stall patterns consisting of one to five zones were found over the equivalent speed range from 5000 to 6200 rpm (about 60 to 75 percent of rated speed).

Maximum vibratory stresses of ±26,400 and ±26,150 psi were measured in the first stage at 5180 rpm and in the second stage at 5860 rpm, respectively. The source of excitation at these two critical speeds was a three-zone rotating stall.

Several cases of nonuniformly spaced and nonuniform-amplitude stall zones were observed. Blade vibrations resulting from these stall patterns were found to be as high as ±16,500 psi. In addition, some hot-wire traces showing the flow patterns during a compressor surge pulse indicated that a single-zone stall pattern occurred just prior to surge.

INTRODUCTION

The excitation of axial-flow-compressor blade vibration by rotating stall has become a serious problem in production compressors. References 1 and 2 indicated that, when a compressor stalls, the annular flow pattern consists of low-flow zones distributed about the annulus and rotating at approximately one-half compressor speed. The existence of the rotating stall has made it possible to explain the source of excitation of blade vibration heretofore referred to as aerodynamically excited. Axial-flow-compressor blade vibrations excited by rotating stall are reported in references 1 to 4.

The vibration survey reported in reference 1 was conducted to determine the cause of the first-stage blade failures occurring in a 13-stage production compressor. The survey indicated that a serious vibration was present in the first-stage rotor and that this vibration was being excited by rotating stall. The first seven rotor stages of this compressor were fabricated from aluminum alloy. Since aluminum has a very low endurance limit, the blades would be susceptible to fatigue failure if moderate vibratory stresses were encountered for a sufficient period of time. The aluminum-bladed compressor was therefore replaced by a design in which the blades in the first three stages were fabricated from a 13-percent-chrome steel. Blade failures were again reported in the steel-bladed compressor. These failures occurred in the blade-root serrations. Since stress determinations in the serrations are difficult to obtain, the present investigation was undertaken to determine whether rotating stall was still an important vibration-exciting influence. The vibratory stress measurements were taken at the base of the airfoil section, where stresses are lower than those in the serrations. A correlation between the stresses in the two locations and a consequent determination of the relation between rotating stall and failure in the blade serrations were left to a subsequent investigation.

Data were obtained at a flight condition that corresponded to an inlet total pressure of 1900 pounds per square foot, an inlet air temperature of 65° F $\pm 5^{\circ}$, and an exhaust pressure of 1800 pounds per square foot. The vibratory stresses were measured by resistance-wire strain gages, and the flow fluctuations of rotating stall were detected by constant-current hot-wire anemometers. Steady-state pressures and temperatures were measured at several stations throughout the compressor. The engine was equipped with a variable-area exhaust nozzle to vary the pressure ratio or air flow at a constant speed.

APPARATUS

Turbojet engine and installation. - The investigation was conducted on a turbojet engine incorporating a 13-stage axial-flow compressor with a pressure ratio of approximately 7, a rated engine speed of 8300 rpm, and an air flow of approximately 120 pounds per second. The engine was installed and operated in an NACA Lewis altitude test chamber. The engine inlet and exhaust pressures were controlled by the laboratory air facilities. The engine was equipped with an adjustable exhaust nozzle to permit variation of the pressure ratio or air flow at a constant speed.

Methods of detecting and measuring vibratory stresses. - Commercial resistance-wire strain gages, used to detect and measure vibratory stresses, were cemented to eight blades in each of the first three compressor stages at approximately midchord position, as close as possible to the blade base. The eight blades per stage were arranged in

two groups of four blades approximately 180° apart. Lead wires were run from the strain gages to a 19-ring slip-ring assembly mounted on the front of the engine starter. The slip-ring assembly and strain-gage circuits were the same as reported in reference 5.

A 24-channel recording oscillograph was used to record the strain-gage and hot-wire anemometer signals.

Hot-wire anemometer. - A constant-current hot-wire anemometer system was used to detect rotating stall. A 0.001-inch-diameter by 0.01-inch-length wire, kept at a constant average temperature, was used in each anemometer. The flow fluctuations were detected from the instantaneous variations in wire temperature. A resistance-capacitor-type compensator was used to obtain the necessary speed of response. Anemometer probes were installed in radial-survey devices located in the first-, second-, and third-stage stator passages.

The anemometer signals were filtered to eliminate frequencies greater than 750 cps. The signal was viewed on a four-beam cathode-ray oscilloscope and recorded with the 24-channel recording oscillograph. The method used to determine the number of stall zones was the same as that used in references 1 and 2. The number of zones per stall pattern and the associated hot-wire frequencies were determined by the angle method of reference 2. Thereafter the hot-wire frequency was used to determine the stall pattern present.

Pressure and temperature instrumentation. - The engine performance instrumentation is shown in figure 1. Radial temperature and pressure rakes were installed ahead of the compressor-inlet guide vanes, interstage positions, compressor outlet, and in the exhaust tail pipe. The air-flow characteristics were calculated from the pressure and temperature measurements at station 1. All probes were spaced at area centers of equal annular areas.

PROCEDURE

The engine was operated over a range of speed from approximately 5000 to 8300 rpm with the exhaust nozzle in the open position. The area of the nozzle in the open position was approximately that required for rated conditions at rated speed. At speeds up to approximately 6200 rpm, the engine operating point was varied by the use of the adjustable nozzle. The minimum nozzle area used was limited by one of the following: (1) maximum allowable tail-pipe temperature (1166° F), and (2) the minimum area of the nozzle. At each condition, data were obtained to determine the over-all compressor performance, stage performance, rotating stall, and rotor-blade-vibration characteristics.

The compressor-inlet total pressure was maintained at about 1900 pounds per square foot. The inlet air temperature was 65° F ±5°. A static pressure of 1800 pounds per square foot was maintained at the exhaust by the laboratory exhaust-system facilities.

RESULTS AND DISCUSSION

The data obtained in this investigation are discussed in their relation to the effect of rotating stall on compressor performance and rotor-blade vibration. Peculiarities noted for some of the rotating-stall patterns are shown.

Rotating-stall characteristics. - The performance of the 13-stage compressor used in this investigation is presented in figure 2 as a plot of total-pressure ratio and adiabatic temperature-rise efficiency against equivalent air flow. In order to determine if rotating stall had any effect on compressor performance, over-all compressor and stage data were obtained in the speed range where rotating stall was encountered. The data points along the lower solid line of the compressor map in figure 2 were taken with the exhaust nozzle set to give approximately rated tail-pipe temperature at rated equivalent speed (8300 rpm). The data points along the upper line were taken with the exhaust nozzle set for minimum available area, limiting tail-pipe temperature, or complete compressor stall or surge encountered with a resultant high turbine temperature. Complete compressor stall is defined as a discontinuous drop in circumferentially averaged compressor-discharge pressure and a high exhaust-gas temperature. A surge cycle is defined as complete compressor stall followed by a reversal of the air flow and a subsequent recovery of the compressor-discharge pressure. A more complete description of the phenomenon is contained in reference 6. In addition to the data taken with the exhaust-nozzle positions for the rated and limiting operating lines, various intermediate settings were used to determine the number of different rotating-stall patterns obtainable and to determine the operating points where high vibratory stresses were encountered in the first three rotor-blade rows. Constant-speed curves have been interpolated from the data points shown.

It can be seen from figure 2 that rotating-stall patterns consisting of one, three, four, or five stall zones could be obtained from about 60 to 75 percent of rated speed (5000 to 6200 equivalent rpm). No rotating stall was encountered at equivalent speeds above approximately 6200 rpm over the flow range investigated. No attempt has been made to draw distinct regions on figure 2 where a particular stall pattern may be encountered; it was felt that insufficient data were taken to warrant a valid line of demarcation (if such exists) from one stall pattern to another. However, in general, three stall zones were found at the higher values of compressor pressure ratio (closed exhaust nozzle) at any given

speed. At the open nozzle position, five stall zones were found at equivalent speeds between 5000 and 5800 rpm. At higher speed with the open nozzle, the anemometer signal was of low amplitude and nonperiodic in nature. At intermediate nozzle settings, four stall zones were found to exist at about 6100 rpm.

It is interesting to note that at equivalent speeds of about 6000 and 6250 rpm a nonperiodic anemometer signal was obtained. The appearance of this type signal usually indicates that the compressor will operate stall-free with a slight increase in speed (see ref. 4); however, this was not the case with this compressor. Reference 7 presents the results of a rotating-stall investigation on a single-stage compressor in which a region of operation with nonperiodic flow fluctuations was bounded by regions of operation with periodic rotating-stall patterns.

During steady-state operation only two points were found where the stall pattern consisted of a single stall zone. One point occurred at an equivalent speed of approximately 5800 rpm with an intermediate nozzle area, and the other at approximately 6200 rpm with the open nozzle. Both points exhibited stall patterns that alternately changed from one to five stall zones with no perceptible change in the engine operating conditions.

In the speed range of 5800 rpm, there was an indication that the stall pattern observed was a function of the operational procedure. In this region, if the equivalent engine speed was held approximately constant and the exhaust area reduced (sketch (a)), the number of zones per pattern changed from five to three to one. However, this sequence could be changed to five, three, two, one by operating the engine in the following manner (sketch (b)): (1) Operate the engine at an equivalent speed of 5600 rpm with the nozzle open, thus obtaining a five-zone stall as indicated at point a. (2) With engine speed constant, close the exhaust nozzle until a three-zone stall is obtained (point b). (3) With the exhaust-nozzle area constant, increase the engine speed to 5800 rpm (point c). (4) Then, with a constant engine speed, close the exhaust nozzle until a two-zone stall is present (point d). Additional reduction in exhaust area would again produce a single-zone stall.

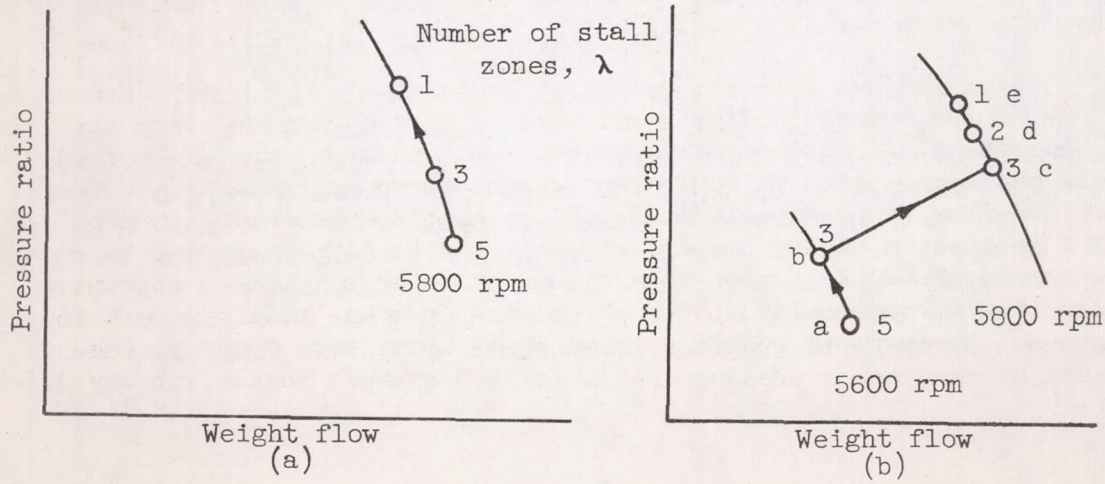

Complete compressor stall, as characterized by a sudden and significant decrease in compressor-discharge pressure and an increase in turbine-inlet temperature, could be attained by rapid engine acceleration. A single stall zone would always be detected at the complete compressor stall, as indicated in references 4 and 6.

The compressor adiabatic efficiencies in figure 2 indicate peak values ranging from 73 percent at an equivalent speed of 5000 rpm to 83 percent at 6200 rpm.

Stage performance. - In addition to the over-all compressor performance measurements, data were obtained at the exits of the second, fourth, and ninth stages. These data are presented in figure 3 as plots of pressure coefficient and temperature-rise coefficient against flow coefficient. These parameters are derived in reference 8 and are used herein as follows (the symbols are defined in the appendix):

$$\text{Flow coefficient} = \phi = \frac{K_1 W_a T_1}{P_1 N}$$

where

$$K_1 = \frac{60R}{\pi D_m A}$$

$$\text{Pressure coefficient} = \psi = \frac{K_2 T_1 \left[\left(\frac{P_3}{P_1} \right)^{\frac{\gamma-1}{\gamma}} - 1.0 \right]}{N^2}$$

$$\text{Temperature-rise coefficient} = \frac{\psi}{\eta} = \frac{K_2 T_1 \left[\left(\frac{T_3}{T_1} \right) - 1.0 \right]}{N^2}$$

where

$$K_2 = \frac{(3600) g J}{n (\pi D_m)^2} c_p$$

The performance of the first stage group, consisting of stages 1 and 2, is shown in figure 3(a). At high speed (near rated), the flow coefficient is high and the pressure and temperature-rise coefficients low. As speed is decreased, the flow coefficient decreases and the pressure and temperature coefficients increase. (It should be remembered that the angle of attack varies inversely with flow coefficient.) The pressure coefficient increases to a maximum of 0.396; then, a slight

decrease in flow coefficient results in rotating stall. Further decrease in flow coefficient results in a decreasing pressure coefficient and an increase in temperature-rise coefficient. Inasmuch as the stage group efficiency is the ratio of pressure coefficient to temperature coefficient, the stage efficiency is decreasing for flow coefficients below 0.425.

The performance of the second-group stages (3 and 4) and third-group stages (5 to 9) is presented in figure 3(b) and (c), respectively. The general trend of change in flow coefficient with respect to change in engine speed is similar to that of the first group; decreasing speed results in decreasing flow coefficient and increasing angle of attack. In the last group (stages 10 to 13) the trend is reversed (fig. 3(d)). As compressor speed is decreased, the angles of attack decrease as indicated by the increased flow coefficients.

These trends can be explained by consideration of the annulus area variation through the compressor. The area variation is determined by the density ratio and axial-velocity ratio through the compressor at design speed and flow operation. As speed is decreased, the density ratio across the compressor decreases rapidly. Since the area ratio cannot be changed, the axial-velocity ratio must increase. Therefore, the angles of attack in the latter stages of the compressor decrease as speed decreases (flow coefficient increases). The low angles of attack in the latter stages combined with the high axial velocities result in a choking condition in the blade passages of the exit stages. This flow limit with decreasing speed causes the inlet flow to decrease more rapidly than the compressor speed. Therefore, the flow coefficient for the inlet stages will decrease and the angles of attack will increase. At some speed then, the inlet stages will reach stall angle of attack, and rotating stall will be generally encountered.

In this particular compressor, rotating stall is encountered at equivalent speeds below about 6200 rpm (about 75 percent of rated speed), and stall-excited blade vibrations may be expected below this speed.

Rotor-blade vibrations. - In figure 4 the relative stall frequency, the average static blade fundamental frequency corrected for the effect of centrifugal force (ref. 9), and the measured frequency at which the blade was found to be vibrating are plotted against the actual engine speed. The frequency of excitation due to rotating stall for rotor blades is termed the relative stall frequency, or the stall frequency relative to the rotor blades, which is defined by the following formula:

$$f_s' = \frac{N\lambda}{60} - f_s$$

Lines representing the relative stall frequency for one- to five-zone stall patterns are presented in the lower half of figure 4. The various patterns were obtained by varying the exhaust-nozzle area, which caused the compressor to operate at various points on the performance map (fig. 2). The two lines A and B represent frequencies that are twice the relative stall frequencies of the four- and three-zone stall patterns, respectively.

The first-stage measured blade-vibration frequencies (fig. 4) follow line B in the speed range from 5000 to 5400 rpm, and the second-stage frequencies follow line B for speeds from 5600 to 6150 rpm. The blades were therefore vibrating at a frequency twice the relative stall frequency of three-zone stall and deviating from their own natural frequency; that is, the blades were being forced to vibrate by the rotating stall. However, this was true only when the relative stall frequency was within approximately 10 cycles of the blade natural frequency. Above 5400 rpm, the rotating stall was unable to force the first-stage blades to vibrate, and they vibrated at frequencies corresponding to their corrected natural frequency.

The third-stage measured blade-vibration frequencies follow line A in the speed range from 5075 to 5450 rpm, and as the speed is increased the blade-vibration frequencies follow their corrected average natural frequencies. Resonance between the rotor blades and rotating stall, or the resultant maximum vibratory stresses, would be expected to occur at the intersection of the rotor-blade and rotating-stall frequency lines. The intersections of these frequency lines were at actual engine speeds of approximately 5200, 5850, and 5300 rpm for the first, second, and third stages, respectively. Figure 5 is a plot of vibratory stress against actual engine speed for the resonant condition.

A peak vibratory stress of ±26,400 psi was observed in the first stage at 5180 rpm (fig. 5(a)). As expected, the maximum stress occurred at the intersection of the rotor-blade frequency line and line B (fig. 4). A stress of ±18,700 psi was observed with a one-zone stall pattern.

A maximum vibratory stress of ±26,150 psi was measured in the second stage at 5860 rpm (fig. 5(b)). A three-zone stall pattern was observed with this peak vibration; again, the peak vibration occurred at the intersection of the blade and relative-stall frequency lines.

The maximum third-stage vibratory stress of ±16,100 psi was excited by a four-zone stall pattern and occurred at 5180 rpm (fig. 5(c)). This critical speed also corresponds to the intersection of the blade and relative-stall frequency lines in figure 4.

Rotating stall was not the source of excitation for all blade vibrations measured. Figure 6, a plot of vibratory stresses not in

resonance with rotating stall against actual engine speed, indicates the blade location and number of zones per stall pattern for each data point. These data points were not presented in figure 5. The maximum nonresonant stresses measured in the first, second, and third stages were ±20,200, ±16,200, and ±16,150 psi, respectively. The blade-vibration and rotating-stall frequencies for these data points did not correlate; that is, the relative stall frequencies, or their harmonics, were not close enough to the blade frequencies for forced excitation.

Rotating-stall patterns. - The annular flow region of the first stages in an axial-flow compressor often consists of normal flow areas with localized low-flow zones if the compressor is operating in the range from 50 to 80 percent of rated speed. These low-flow, or stalled, zones have generally been considered to be approximately evenly spaced and of equal strength or size. The annular pattern is referred to as a rotating stall, or stall, pattern. During this investigation stall patterns were observed where the spacing of the zones was nonperiodic and where the strength or size of the zones varied. Figure 7 shows the hot-wire anemometer signal for a periodic and uniform three-zone rotating-stall pattern. A sketch of the annulus, illustrating the location of the stall zones, is also shown. It can be seen from the hot-wire signals that these stall zones are equally spaced and of equal size or strength.

Figure 8 shows the continuous hot-wire signal obtained during a transition from a one-zone to a three-zone stall pattern. In this transition several patterns were formed. The compressor speed was constant (6050 rpm) for the duration of this record. In section a (fig. 8), the hot-wire signal shows that a one-zone stall pattern was present. In section b the pattern changed to a four-zone pattern, with the zones alternately weak and strong. At times the weak zones are about one-half the strength of the strong zones; and at other times the weak zones are practically missing, with the hot wires showing the presence of only a two-zone stall. In section c the high peaks represent a one-zone stall pattern and the low peaks a five-zone stall. Section d represents the final transition before the three-zone stall pattern is formed; the spacing is initially very uneven, some of the peaks being spaced as a three-zone pattern and some as four- and five-zone patterns. In section e only a stable periodic three-zone pattern remained. The unevenly spaced stall patterns not only occur during the transition condition from one stable stall pattern to another, but they have been observed as stable patterns exciting blade vibration.

Figure 9 is an oscillograph record of the second- and third-stage vibrations occurring with a three-zone stall pattern where two zones are strong and one weak or missing. The maximum vibratory stress for both stages was approximately ±16,500 psi. For the second stage the ratio of the blade frequency to the relative stall frequency was 2.00; however, for the third stage it was 2.33.

In figure 10 the second-stage blades are shown vibrating at a maximum vibratory stress of ±16,770 psi with a four-zone stall pattern such as shown in section b of figure 8, that is with alternately strong and weak zones. The frequency ratio, based on only the two strong peaks in the pattern, is 3.0; thus, rotating stall is probably the source of these vibrations.

Figure 11 shows the second stage vibrating at a maximum vibratory stress of ±13,080 psi with the one- and five-zone pattern, such as in section c of figure 8. The high peaks correspond to a single stall zone and the low peaks to a five-zone stall pattern. The ratio of the blade frequency to the relative stall frequency for the one-zone stall was 6.0.

Figure 12 presents the hot-wire signal of rotating stall as the number of zones is changing from three to one. In section a the second stage was vibrating at a maximum stress of ±16,350 psi and was excited by a three-zone stall pattern. In section b the blade vibratory stresses were decreasing, and an examination of the hot-wire signals shows that the stall zones were unevenly spaced. The spacing between the two closest zones was approximately 90° and the other two spacings were each 135°. Approximately 0.2 second after this stall spacing formed, the number of zones changed from three to one; and approximately 0.3 second after the one-zone spacing formed, the first stage started to vibrate at a maximum vibratory stress of ±15,100 psi (section c). The ratio of stall frequency to blade frequency at this point was 5.0.

The hot-wire anemometer signal reproduced in figure 13 illustrates the flow pattern in the compressor as the compressor stall pattern changes from a single-zone pattern to a surge or axial pulsing of the air. The frequency of the one-zone pattern was approximately 41 cps and of the surge cycle was 9 cps. It can be noted that as the compressor recovered from each surge cycle the single-zone stall pattern returned. It thus appeared that, with this compressor, single-zone stall was the prelude to surge. The vibratory stresses for the duration of this record were within ±5,000 psi. The vibration was the bursting type; that is, the blades would vibrate for 25 or 30 cycles and then cease.

SUMMARY OF RESULTS

A vibration survey was conducted on a 13-stage axial-flow compressor to determine the source of excitation of the destructive blade vibration reportedly causing compressor failures. Strain gages and hot-wire anemometers were used to detect the blade vibration and rotating stall, respectively. The results may be summarized as follows:

1. The compressor was operating with rotating stall at equivalent speeds below about 6200 rpm (75 percent of rated speed). Stall patterns consisting of one to five stall zones were found.

2. In general, the number of stall zones in the annulus decreased as the exhaust nozzle was closed at any given engine speed.

3. The single stall zone usually occurred just prior to compressor surge.

4. The maximum compressor efficiencies, measured while rotating stall was present, ranged from 73 percent at an equivalent speed of 5000 rpm to 83 percent at an equivalent speed of 6200 rpm.

5. The stage performance data indicated that the flow coefficient for the first nine stages decreased with decreasing speed and increased with decreasing speed in the last four stages.

6. The first-stage peak vibratory stress of ±26,400 psi, measured at the airfoil base at 5180 rpm, was caused by a three-zone rotating stall.

7. The second-stage peak vibratory stress of ±26,150 psi, measured at the airfoil base at 5860 rpm, was caused by a three-zone rotating stall.

8. The third-stage peak vibratory stress of ±16,100 psi, measured at the airfoil base at 5180 rpm, was caused by a four-zone rotating stall.

9. Vibratory stresses of ±20,200, ±16,200, and ±16,150 psi that could not be correlated with rotating stall were measured in the first, second, and third stages, respectively.

Lewis Flight Propulsion Laboratory
National Advisory Committee for Aeronautics
Cleveland, Ohio, October 28, 1954

APPENDIX - SYMBOLS

The following symbols are used in this report:

A annulus area, sq ft

c_p specific heat at constant pressure, Btu/(lb)($^\circ$R)

D_m mean diameter, ft

f_s stall frequency, cps

f_s' stall frequency relative to rotor, cps

g acceleration due to gravity, ft/sec^2

J mechanical equivalent of heat, 778 ft-lb/Btu

$K_1 = \frac{60R}{\pi D_m A}$

$K_2 = \frac{(3600)gJ}{\eta(\pi D_m)^2} c_p$

N engine speed, rpm

n number of stages

P total pressure, lb/sq ft

R gas constant, ft-lb/(lb)($^\circ$R)

T total temperature, $^\circ$R

W_a air flow at compressor inlet, lb/sec

γ ratio of specific heats

δ ratio of pressure to NACA standard sea-level pressure

η adiabatic temperature-rise efficiency, $\eta = \frac{T_1\left[\left(\frac{P_3}{P_1}\right)^{\frac{\gamma-1}{\gamma}} - 1.0\right]}{T_3 - T_1}$

θ ratio of total temperature to NACA standard sea-level temperature

λ number of stall zones

ψ pressure coefficient, $\psi = \dfrac{K_2 T_1 \left[\left(\dfrac{P_3}{P_1} \right)^{\frac{\gamma-1}{\gamma}} - 1.0 \right]}{N^2}$

ϕ flow coefficient, $\phi = \dfrac{K_1 W_a T_1}{P_1 N}$

Subscripts:

c compressor

1 compressor inlet

3 compressor outlet

REFERENCES

1. Huppert, Merle C., Calvert, Howard F., and Meyer, André J., Jr.: Experimental Investigation of Rotating Stall and Blade Vibration in the Axial-Flow Compressor of a Turbojet Engine. NACA RM E54A08, 1954.

2. Huppert, Merle C.: Preliminary Investigation of Flow Fluctuations During Surge and Blade Row Stall in Axial-Flow Compressors. NACA RM E52E28, 1952.

3. Huppert, Merle C., Johnson, Donald F., and Costilow, Eleanor L.: Preliminary Investigation of Compressor Blade Vibration Excited by Rotating Stall. NACA RM E52J15, 1952.

4. Huppert, Merle C., Costilow, Eleanor L., and Budinger, Ray E.: Investigation of a 10-Stage Subsonic Axial-Flow Research Compressor. III - Investigation of Rotating Stall, Blade Vibration, and Surge at Low and Intermediate Compressor Speeds. NACA RM E53C19, 1953.

5. Meyer, André J., Jr., and Calvert, Howard F.: Vibration Survey of Blades in 10-Stage Axial-Flow Compressor. II - Dynamic Investigation. NACA RM E8J22a, 1949. (Supersedes NACA RM E7D09.)

6. Huppert, Merle C., and Benser, William A.: Some Stall and Surge Phenomena in Axial-Flow Compressions. Jour. Aero. Sci., vol. 20, no. 12, Dec. 1953, pp. 835-845.

7. Graham, Robert W., and Prain, Vasily D.: Experimental and Theoretical Investigation of Rotating-Stall Characteristics of Single-Stage Axial-Flow Compressor with Hub-Tip Ratio of 0.76. NACA RM E53I09, 1953.

8. Medeiros, Arthur A., Benser, William A., and Hatch, James E.: Analysis of Off-Design Performance of a 16-Stage Axial-Flow Compressor with Various Blade Modifications. NACA RM E52L03, 1953.

9. Timoshenko, Stephen: Vibration Problems in Engineering. Second ed., D. Van Nostrand C., Inc., 1937, p. 386.

	Type of measurement	Number measurements per station, at station -					
		1	2s	4s	9s	3	9
O	Total pressure	20	5	5	3	12	35
□	Total temperature	12	5	5	3	6	30
△	Wall static pressure	4	-	-	-	-	-
◇	Stream static pressure	4	-	-	-	-	-

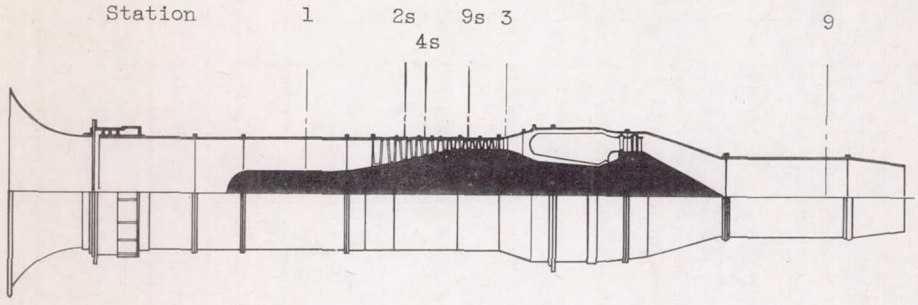

(a) Engine.

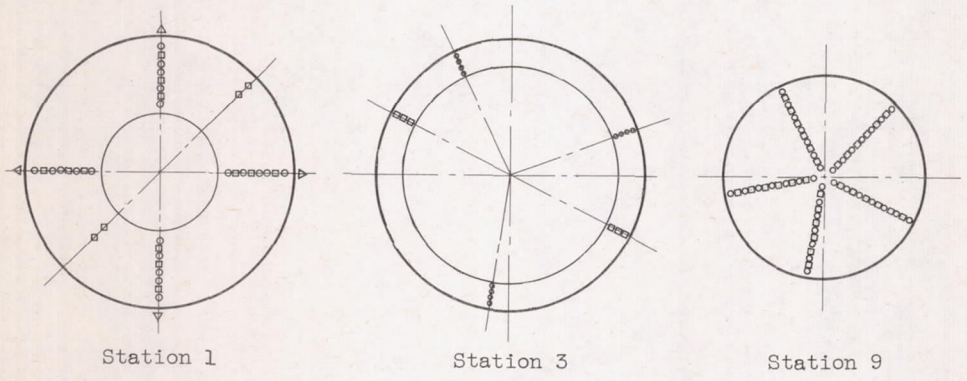

(b) Several stations (viewed downstream).

Figure 1. - Cross section of engine showing instrumentation stations.

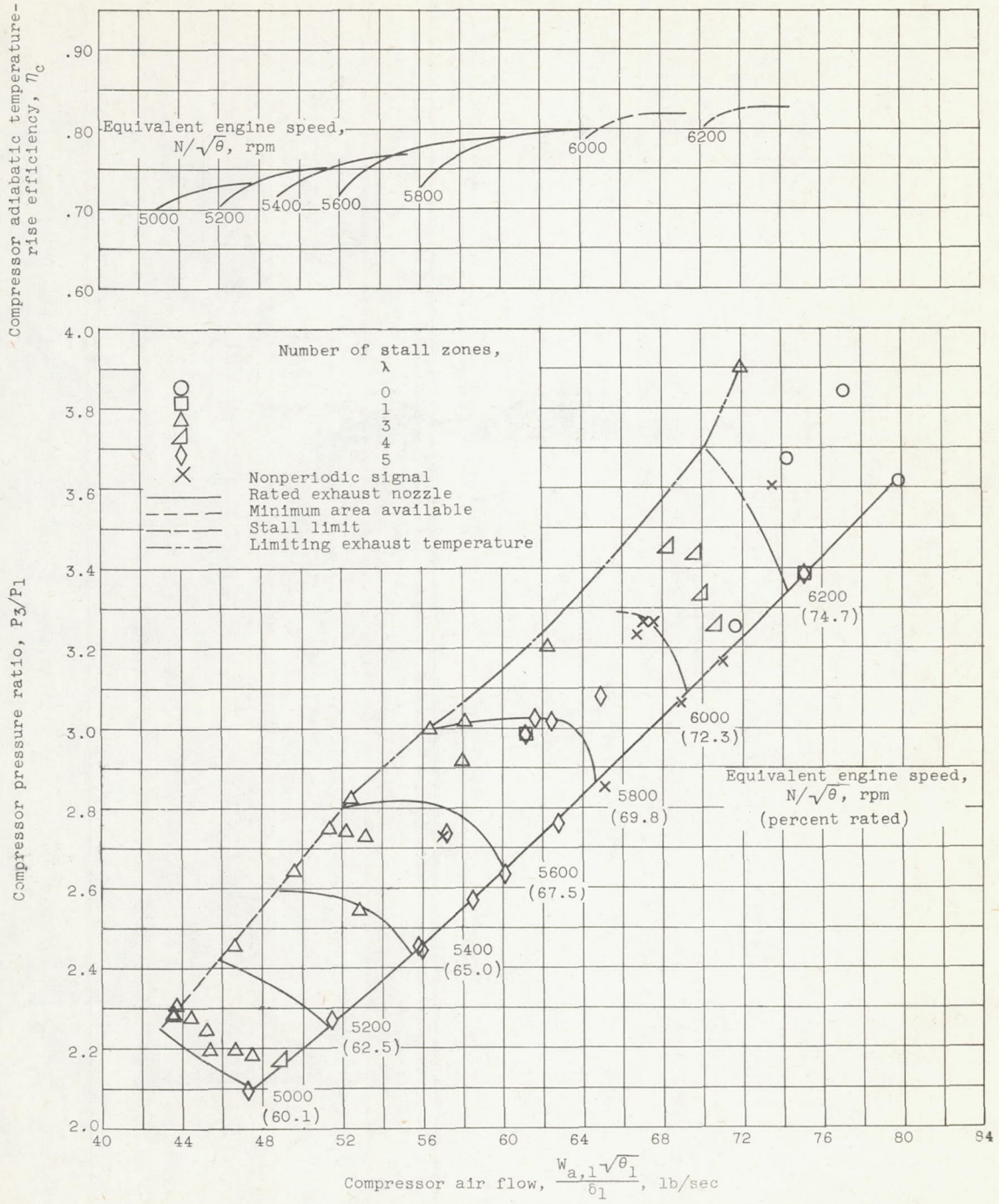

Figure 2. - Over-all performance and rotating-stall characteristics of 13-stage compressor.

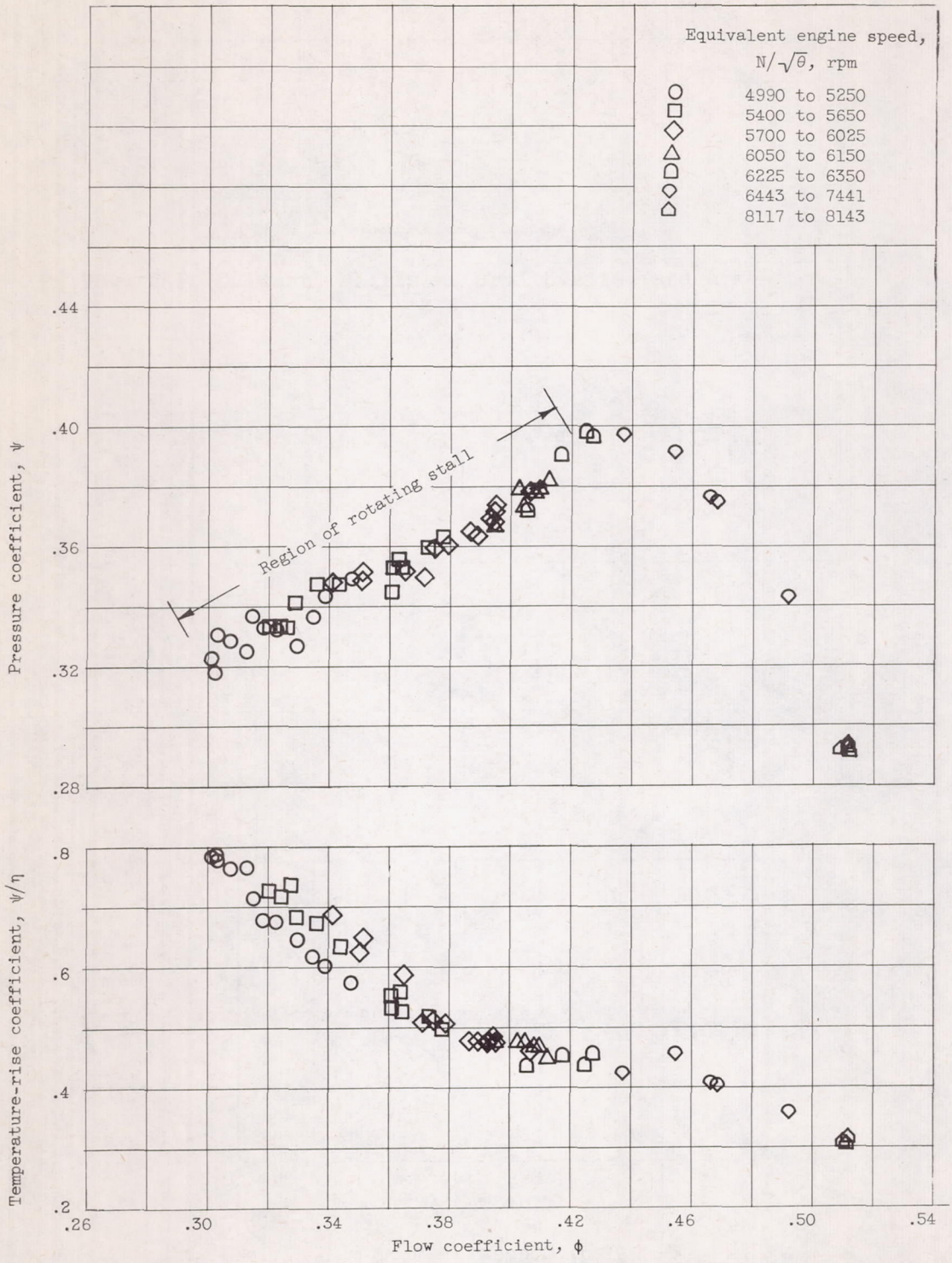

(a) Stages 1 and 2.

Figure 3. - Stage performance characteristics of 13-stage compressor.

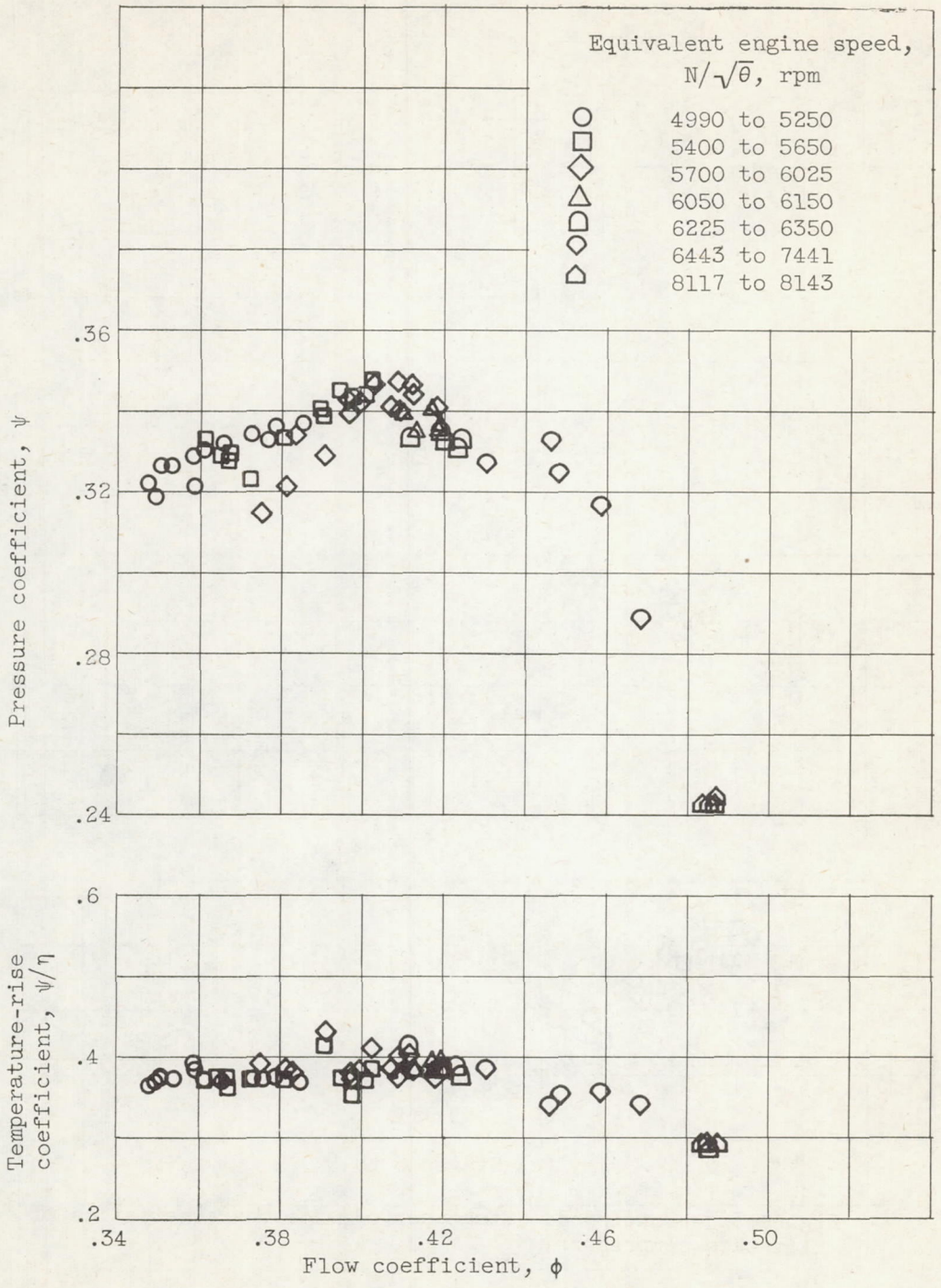

(b) Stages 3 and 4.

Figure 3. Continued. Stage performance characteristics of 13-stage compressor.

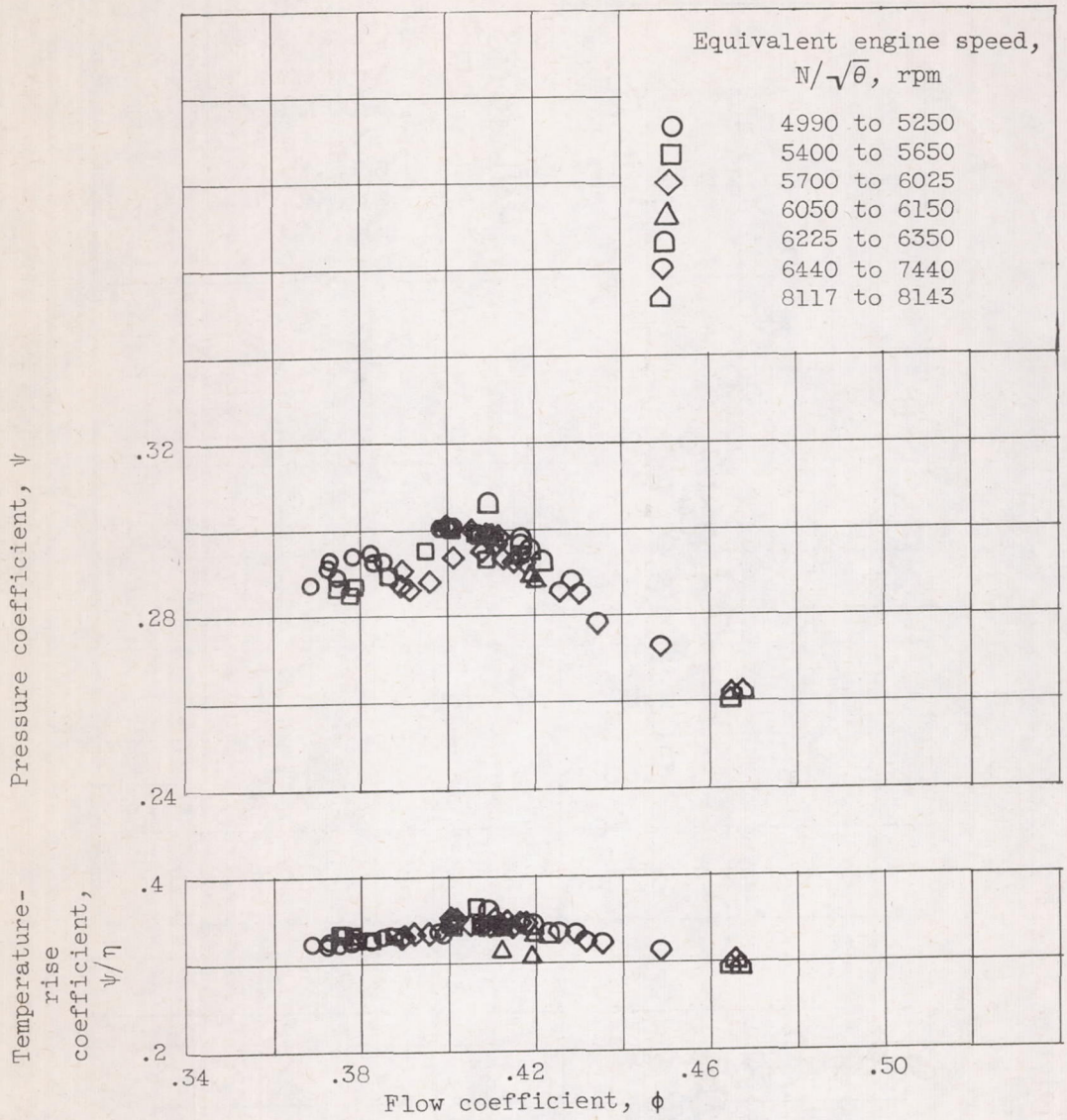

(c) Stages 5 to 9.

Figure 3. - Continued. Stage performance characteristics of 13-stage compressor.

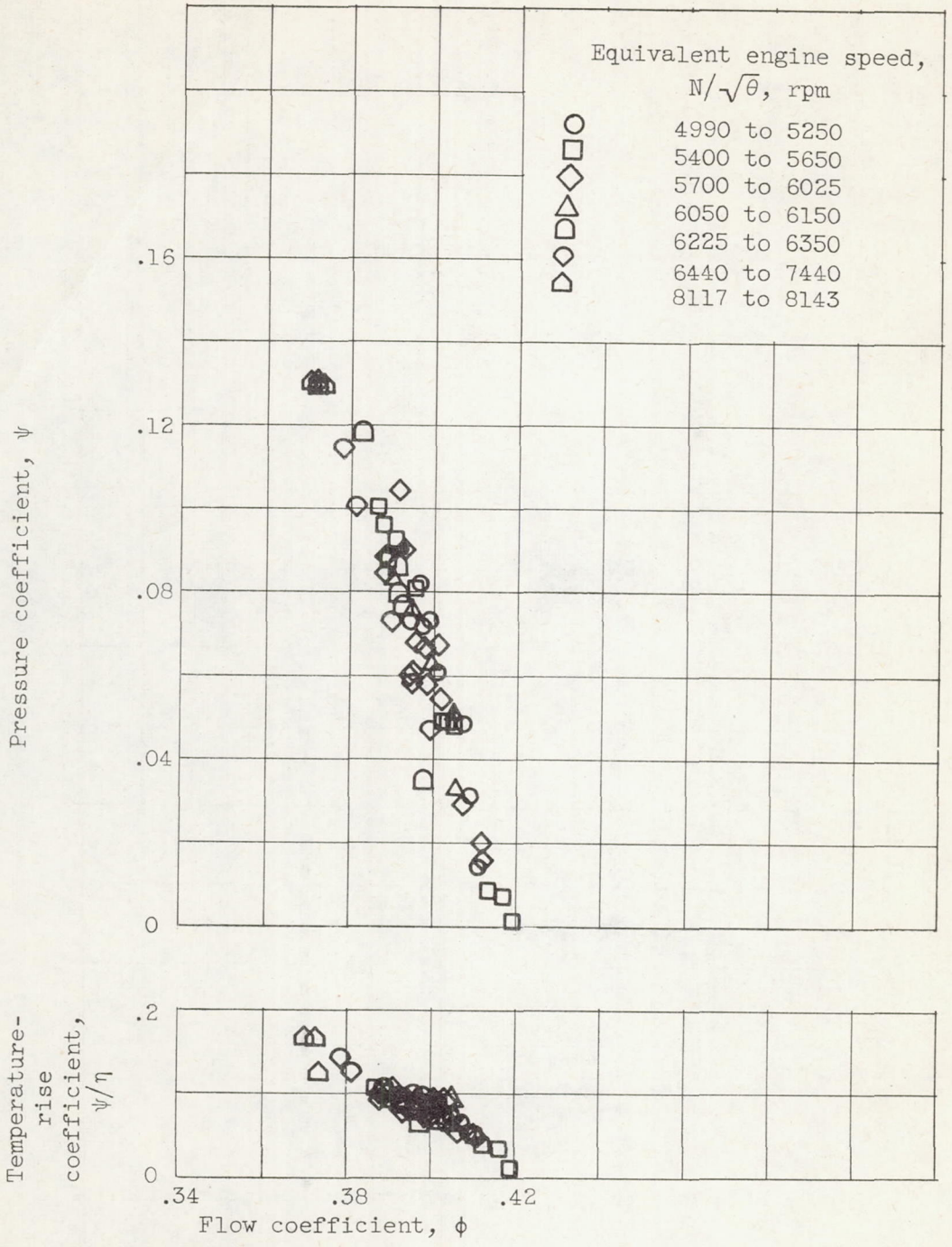

(d) Stages 10 to 13.

Figure 3. - Concluded. Stage performance characteristics of 13-stage compressor.

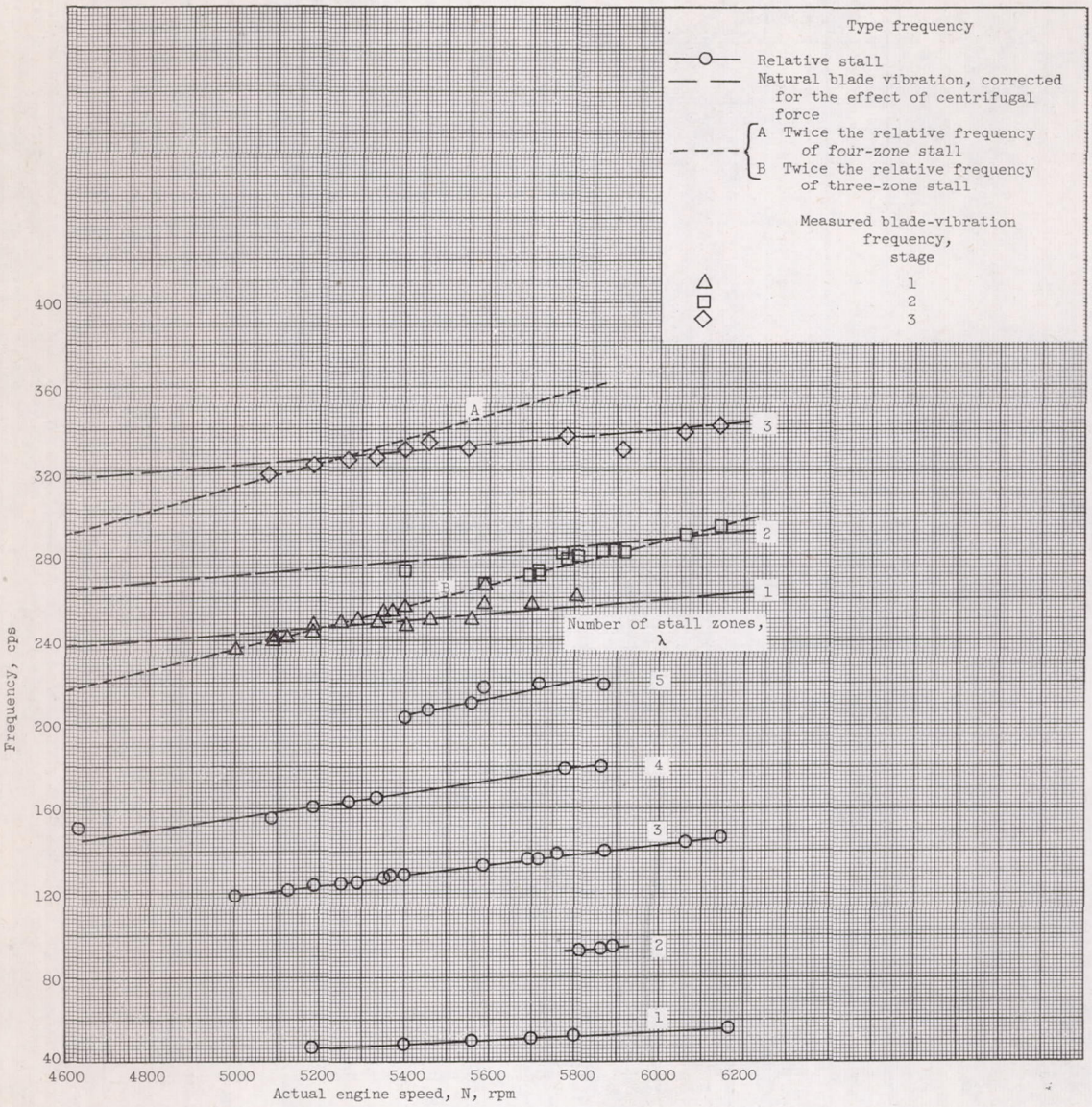

Figure 4. - Stall and blade-vibration frequencies for 13-stage compressor.

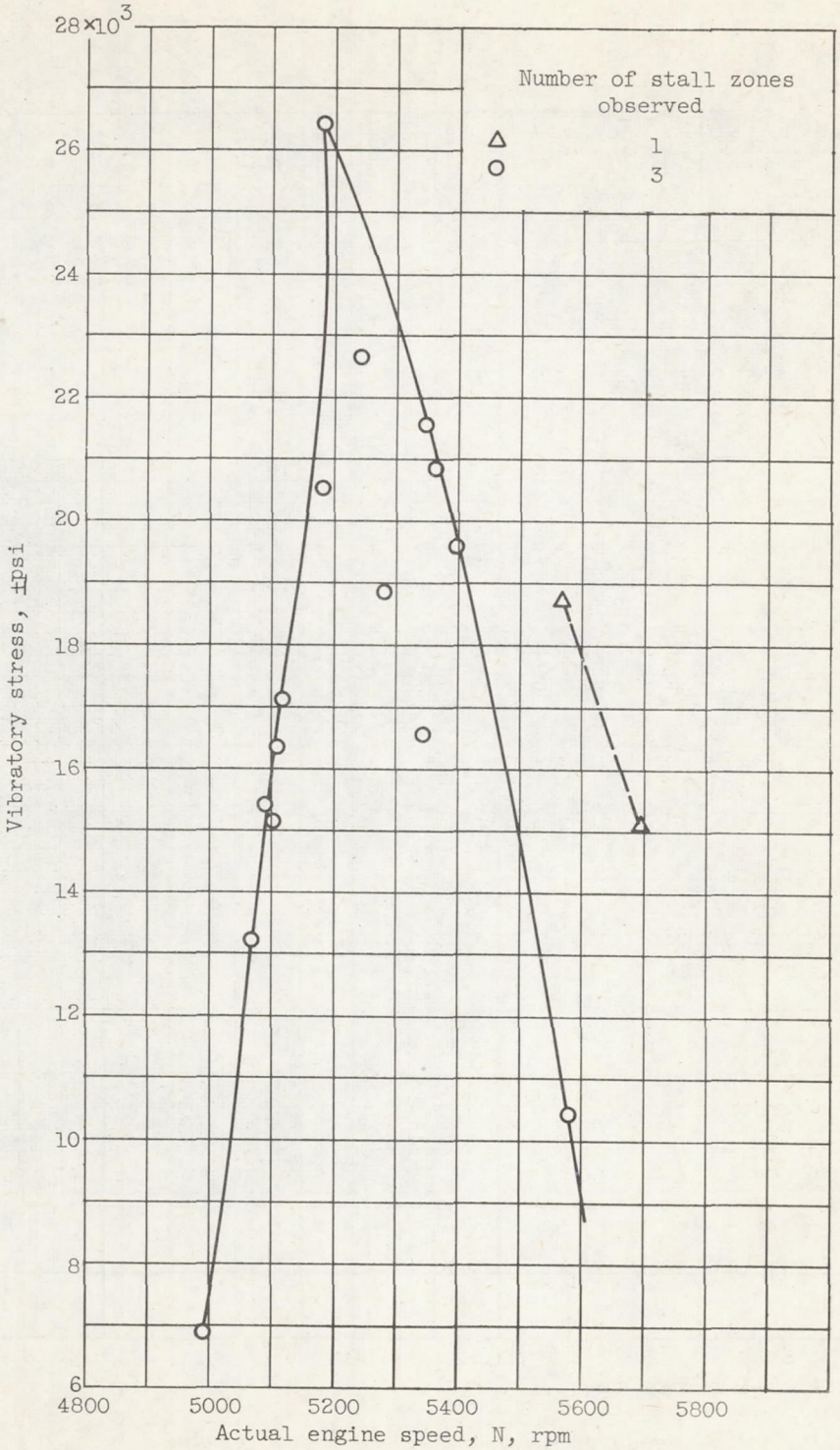

(a) Measured in first-stage rotor blades.

Figure 5. - Resonant vibratory stresses.

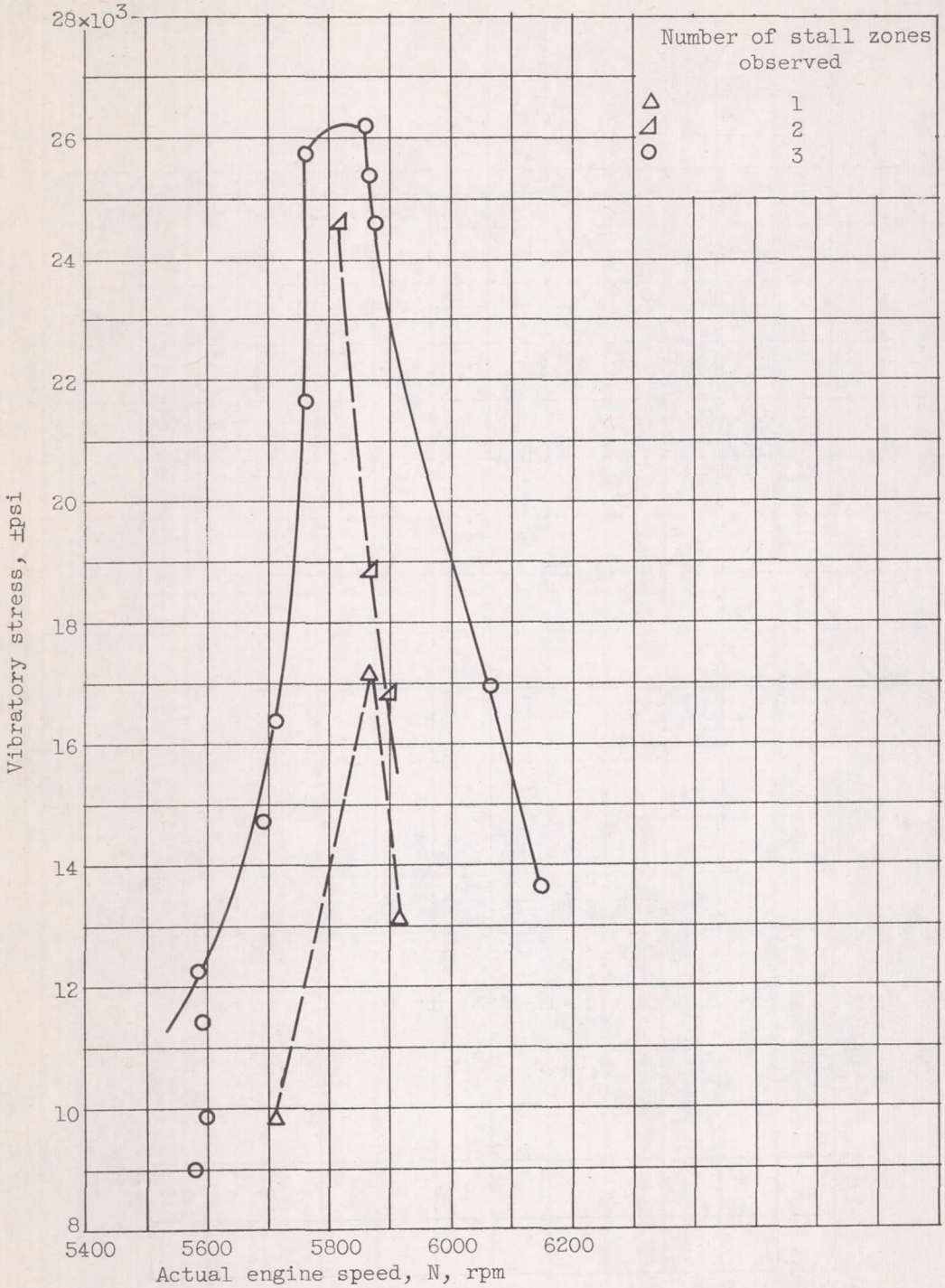

(b) Measured in second-stage rotor blades.

Figure 5. - Continued. Resonant vibratory stresses.

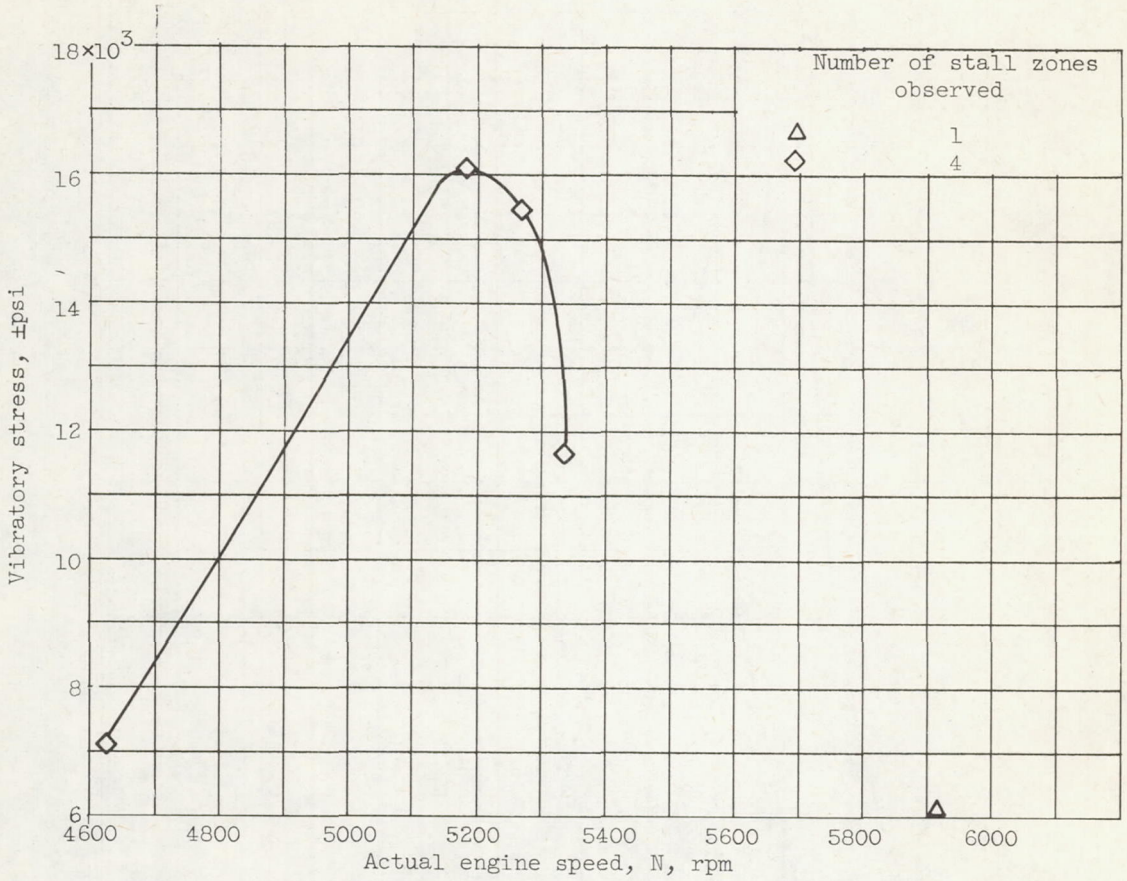

(c) Measured in third-stage rotor blades.

Figure 5. - Concluded. Resonant vibratory stresses.

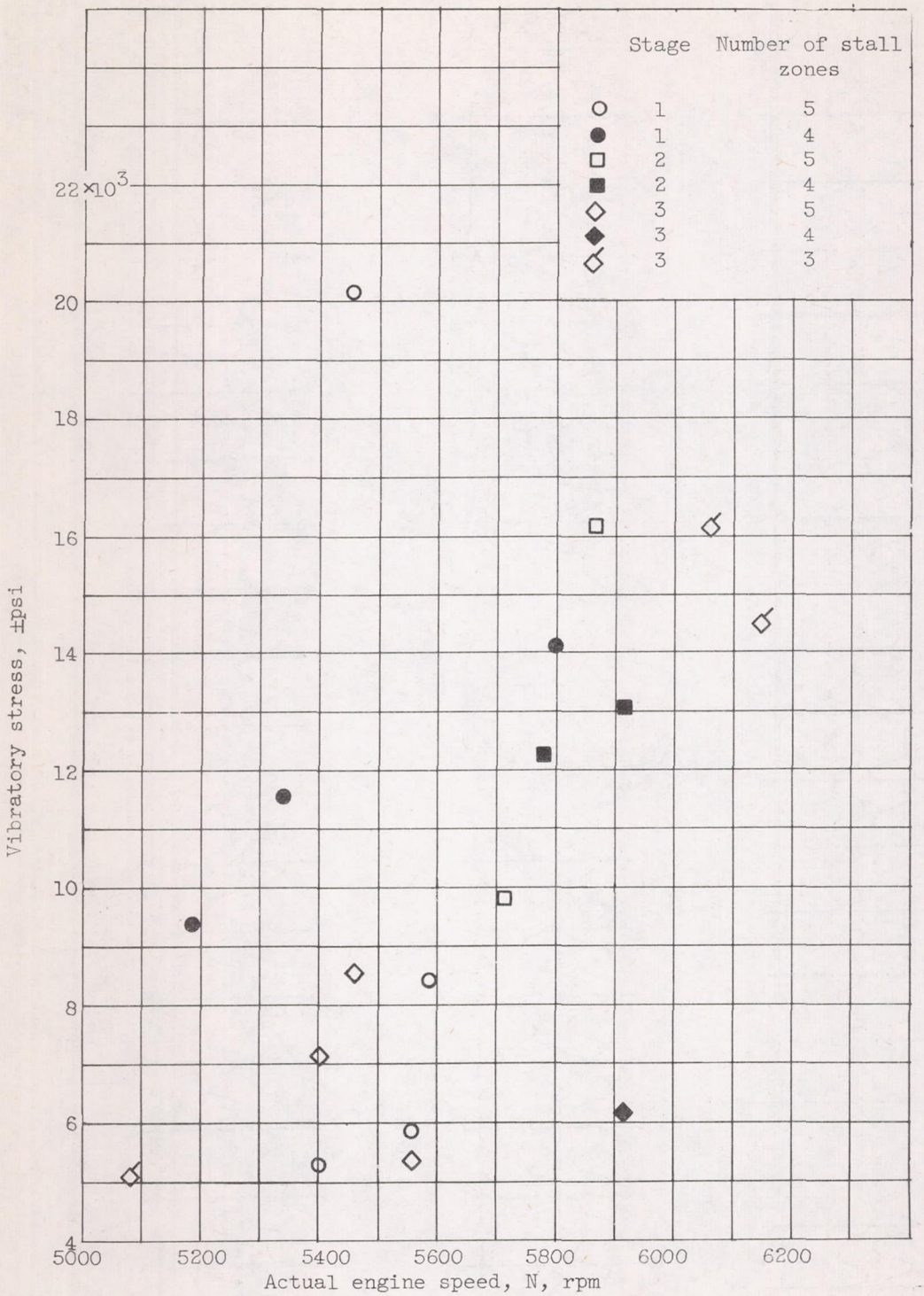

Figure 6. - Vibratory stresses, not in resonance with rotating stall, measured in first three rotor stages.

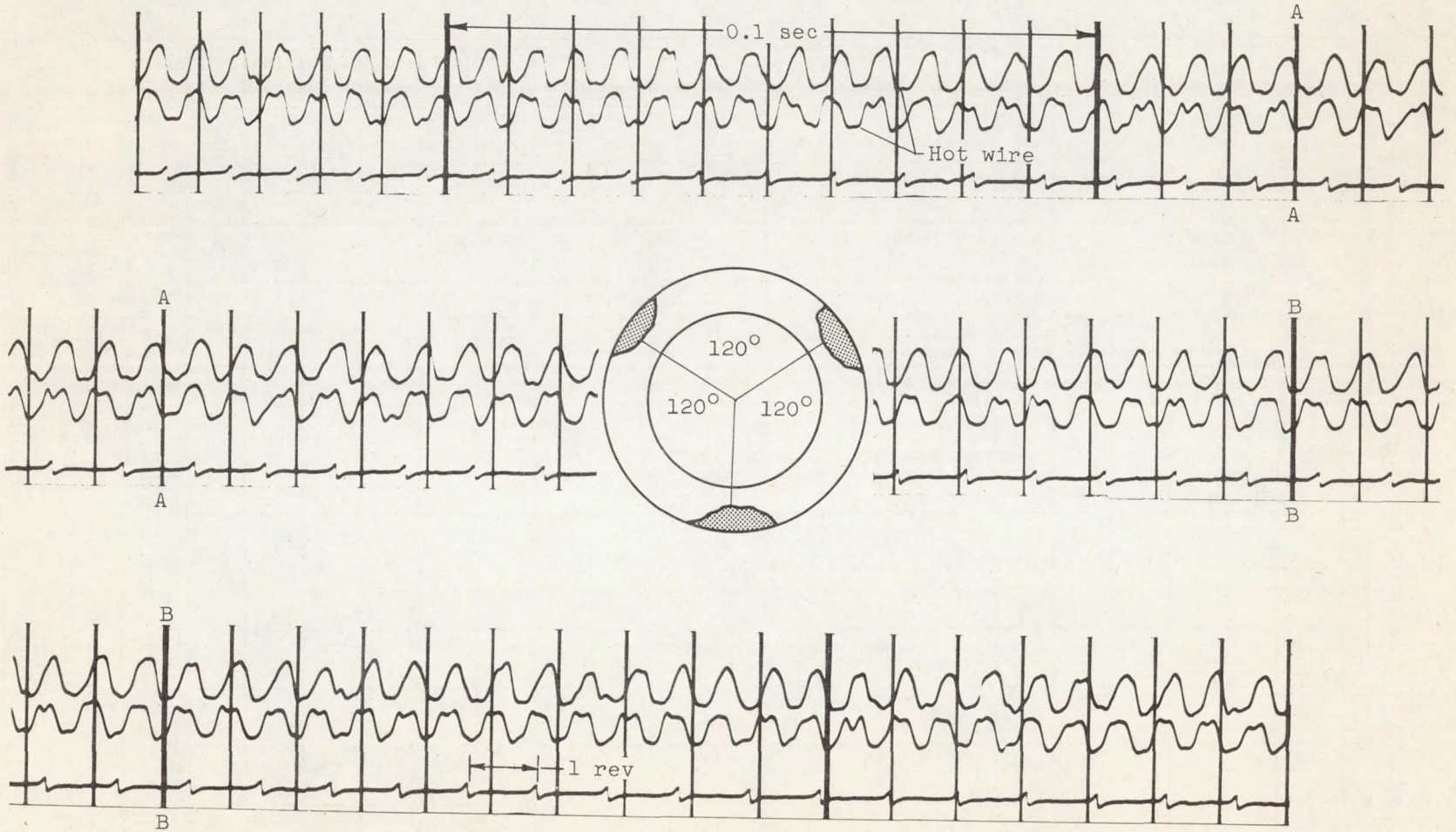

Figure 7. - Hot-wire anemometer signal of periodic and uniform three-zone rotating-stall pattern. Actual engine speed, 5714 rpm.

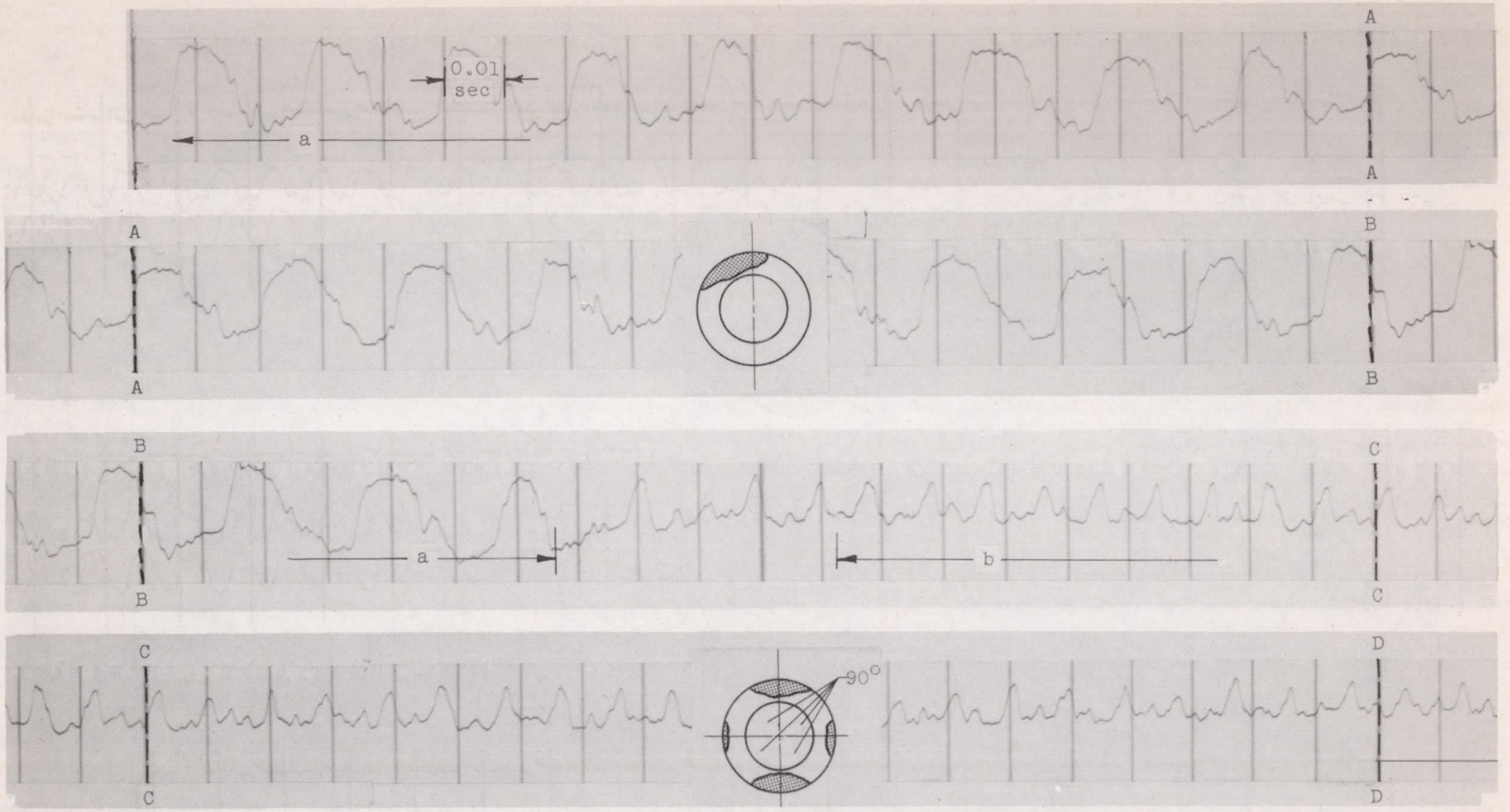

Figure 8. - Hot-wire anemometer signal showing number of zones in a stall pattern changing from one to three zones. Actual engine speed, 6050 rpm.

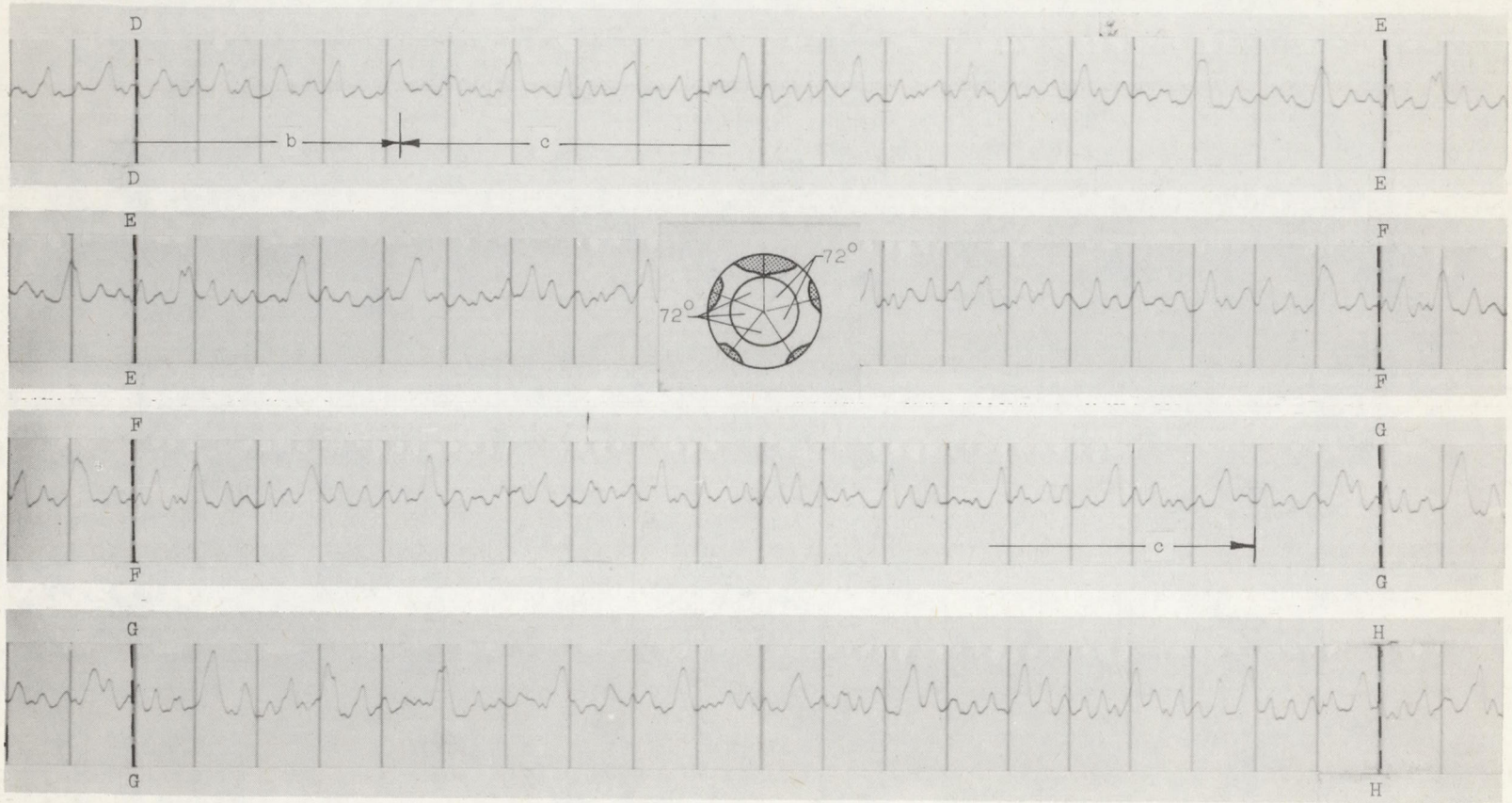

Figure 8. - Continued. Hot-wire anemometer signal showing number of zones in a stall pattern changing from one to three zones. Actual engine speed, 6050 rpm.

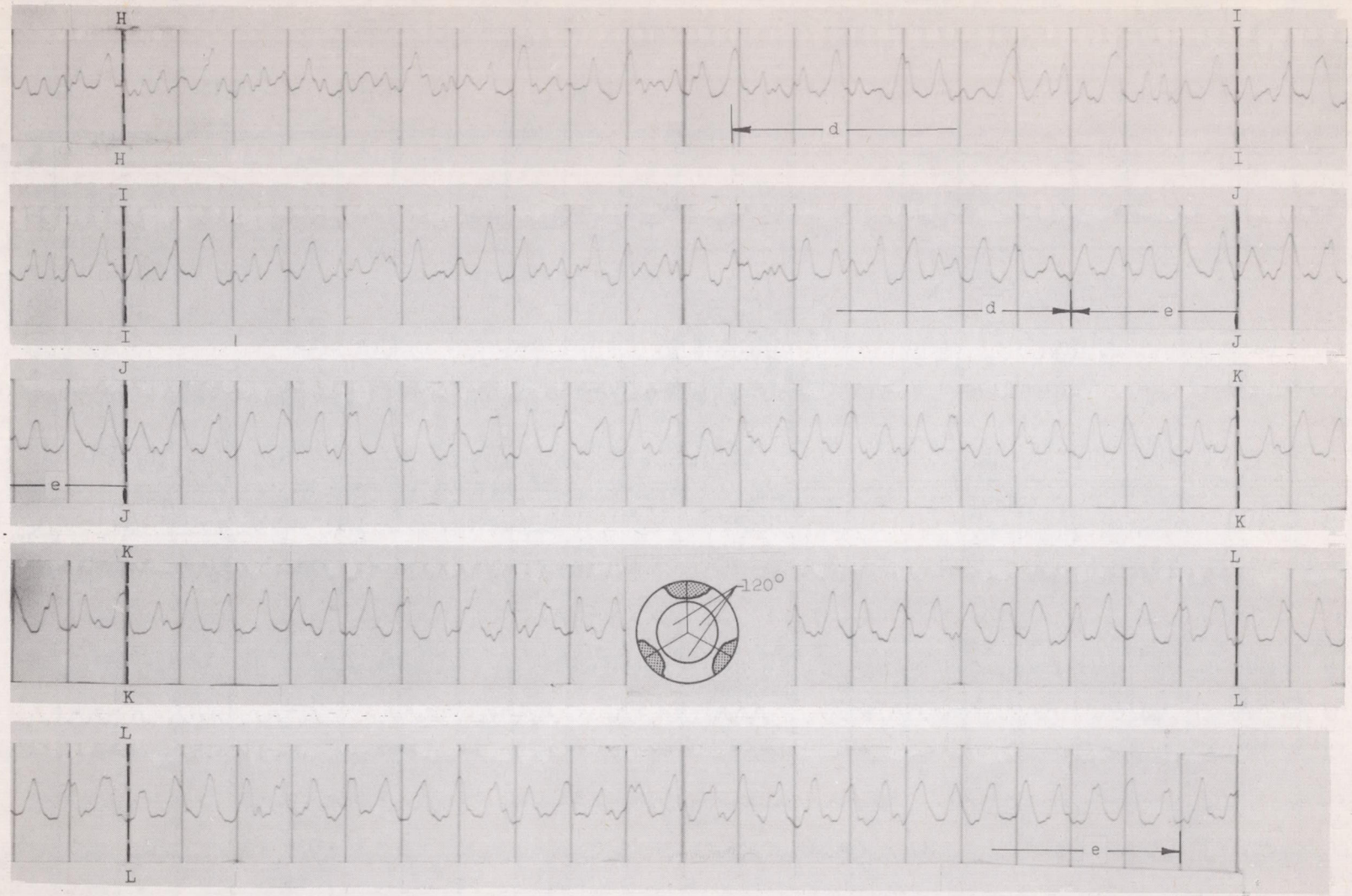

Figure 8. - Concluded. Hot-wire anemometer signal showing number of zones in a stall pattern changing from one to three zones. Actual engine speed, 6050 rpm.

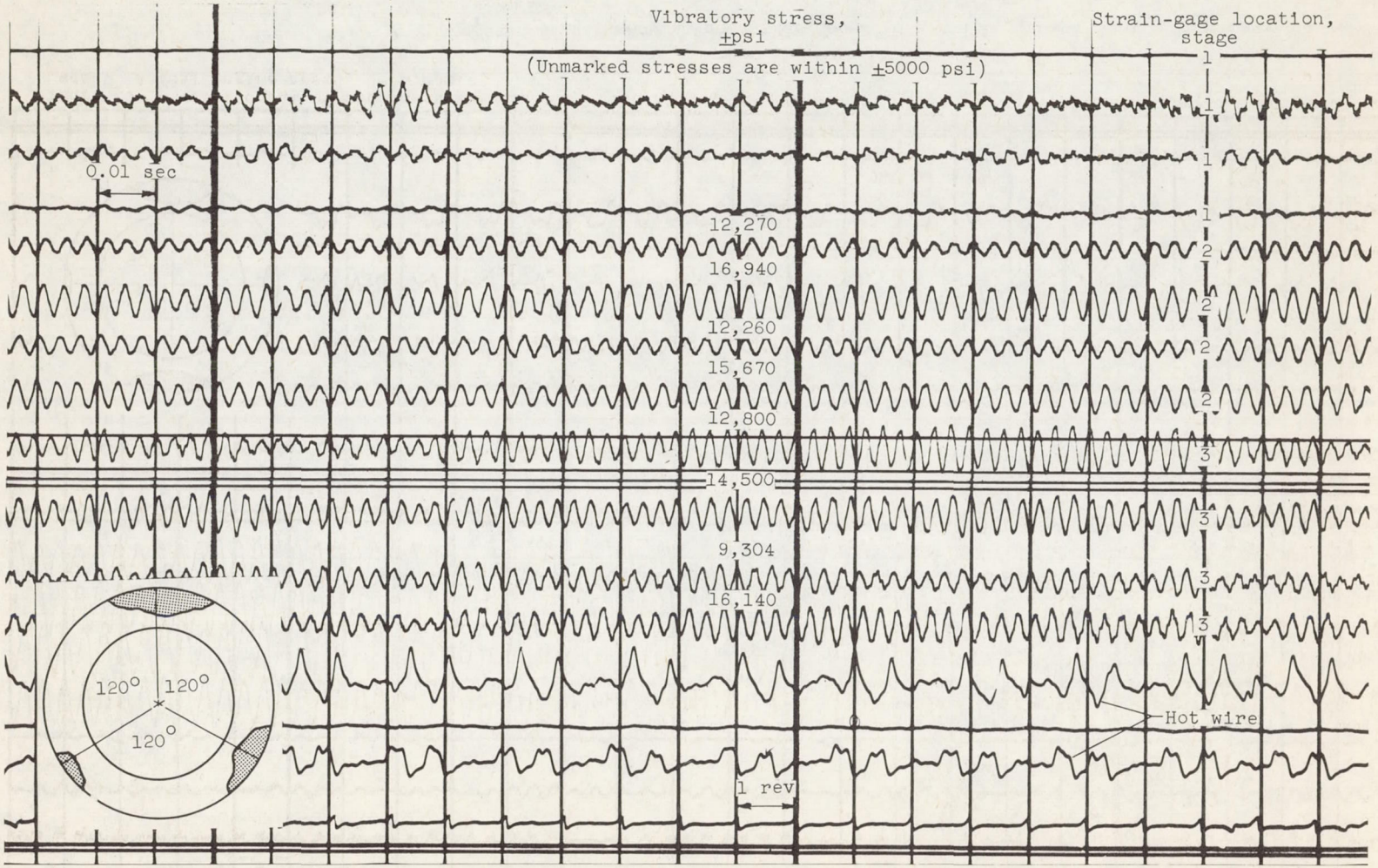

Figure 9. - Oscillogram of second- and third-stage vibration occurring with nonuniform three-zone stall pattern. Actual engine speed, 6060 rpm.

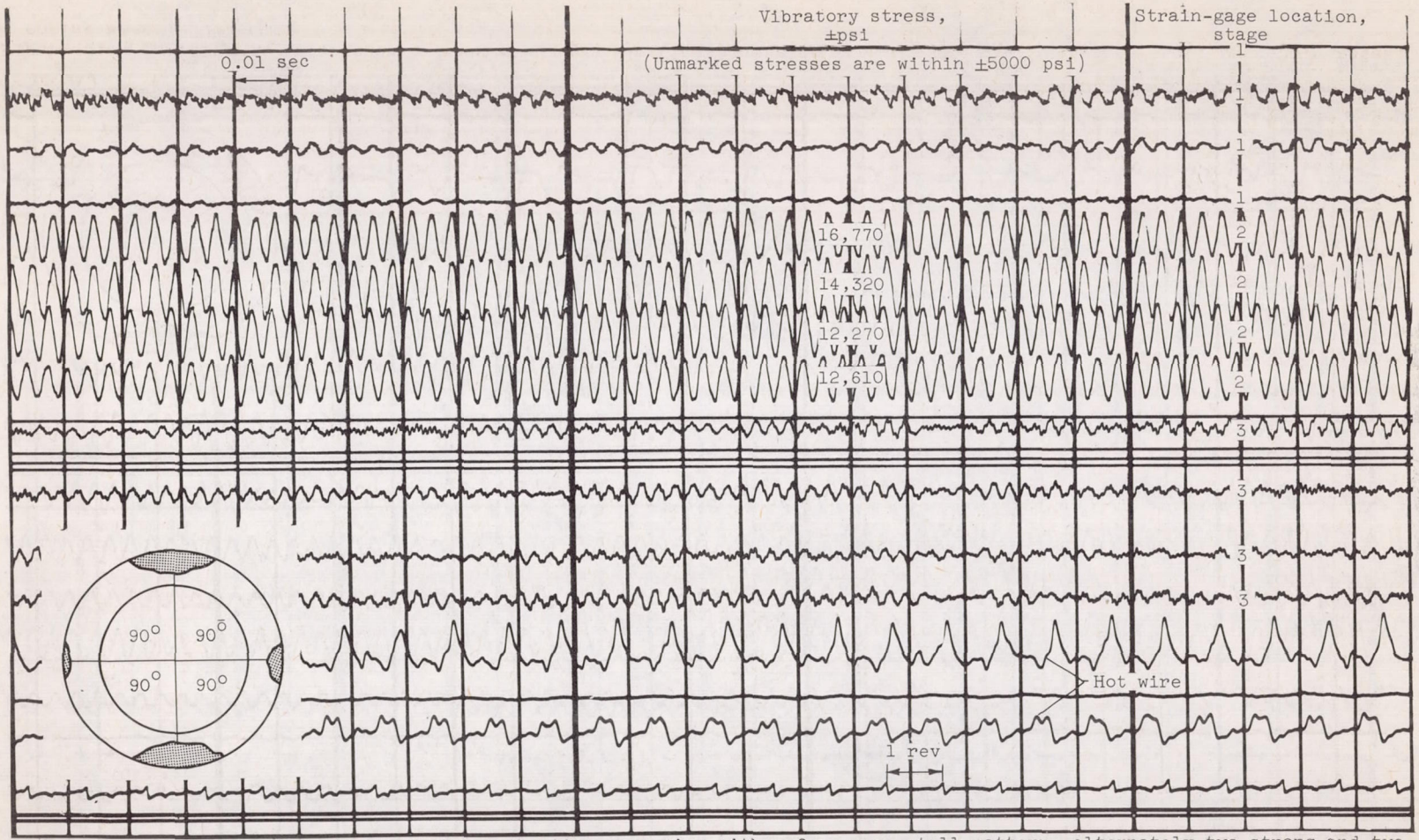

Figure 10. - Oscillogram of second-stage vibration occurring with a four-zone stall pattern, alternately two strong and two weak. Actual engine speed, 5895 rpm.

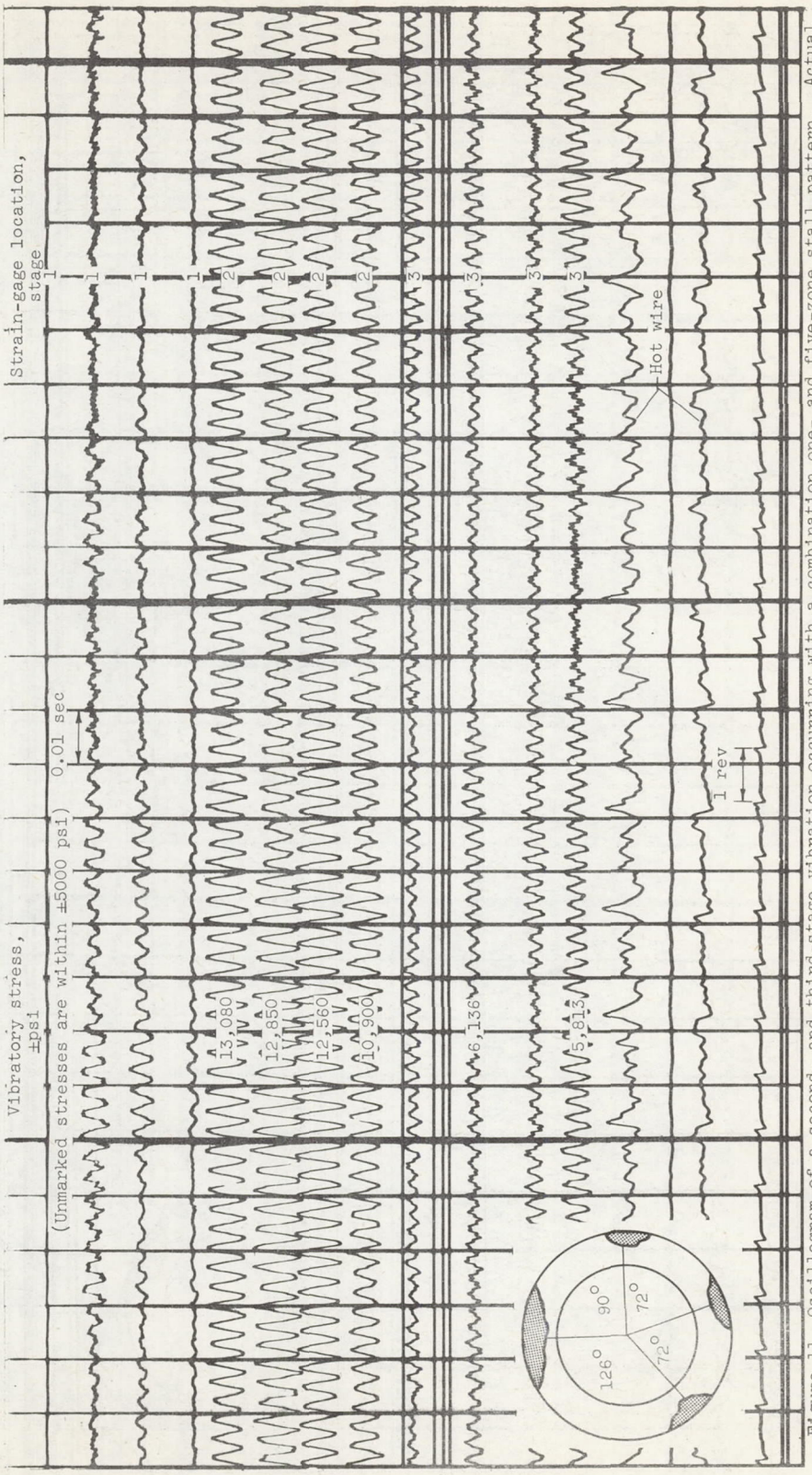

Figure 11. Oscillogram of a second- and third-stage vibration occurring with a combination one- and five-zone stall pattern. Actual engine speed, 5915 rpm.

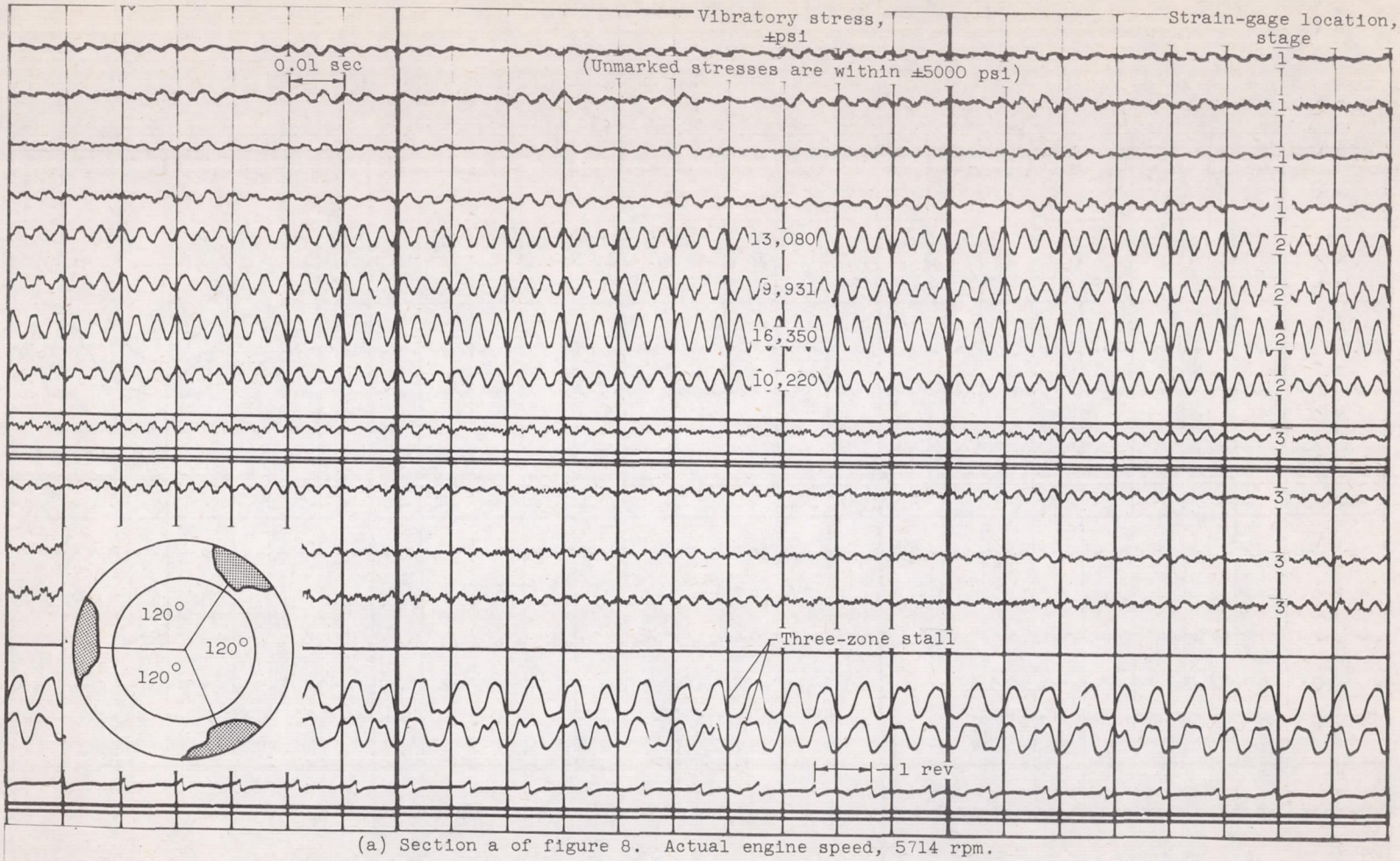

(a) Section a of figure 8. Actual engine speed, 5714 rpm.

Figure 12. - Oscillogram showing effect of changing the number of zones per stall pattern from three to one on first- and second-stage blade vibration.

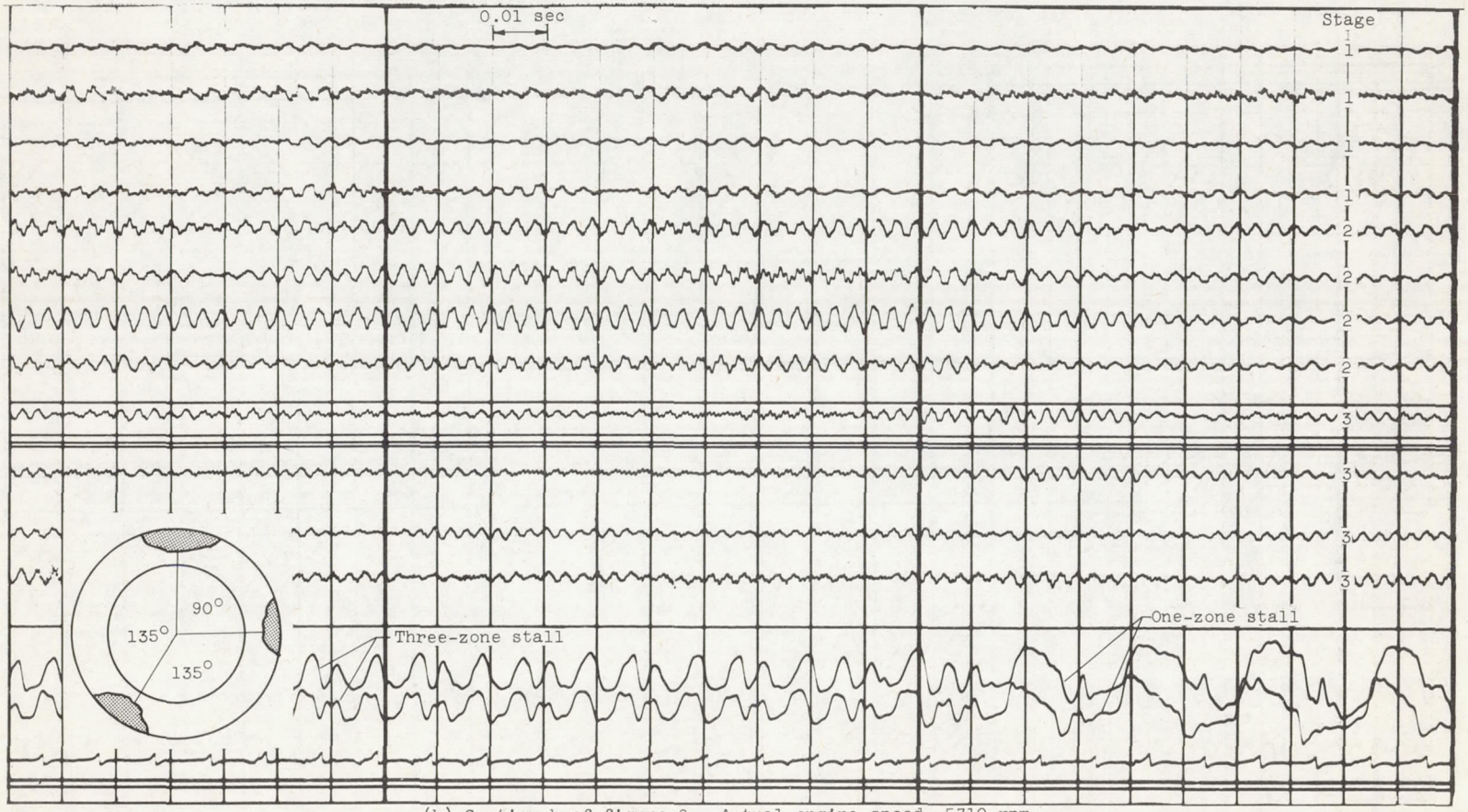

(b) Section b of figure 8. Actual engine speed, 5710 rpm.

Figure 12. - Continued. Oscillogram showing effect of changing the number of zones per stall pattern from three to one on first- and second-stage blade vibration.

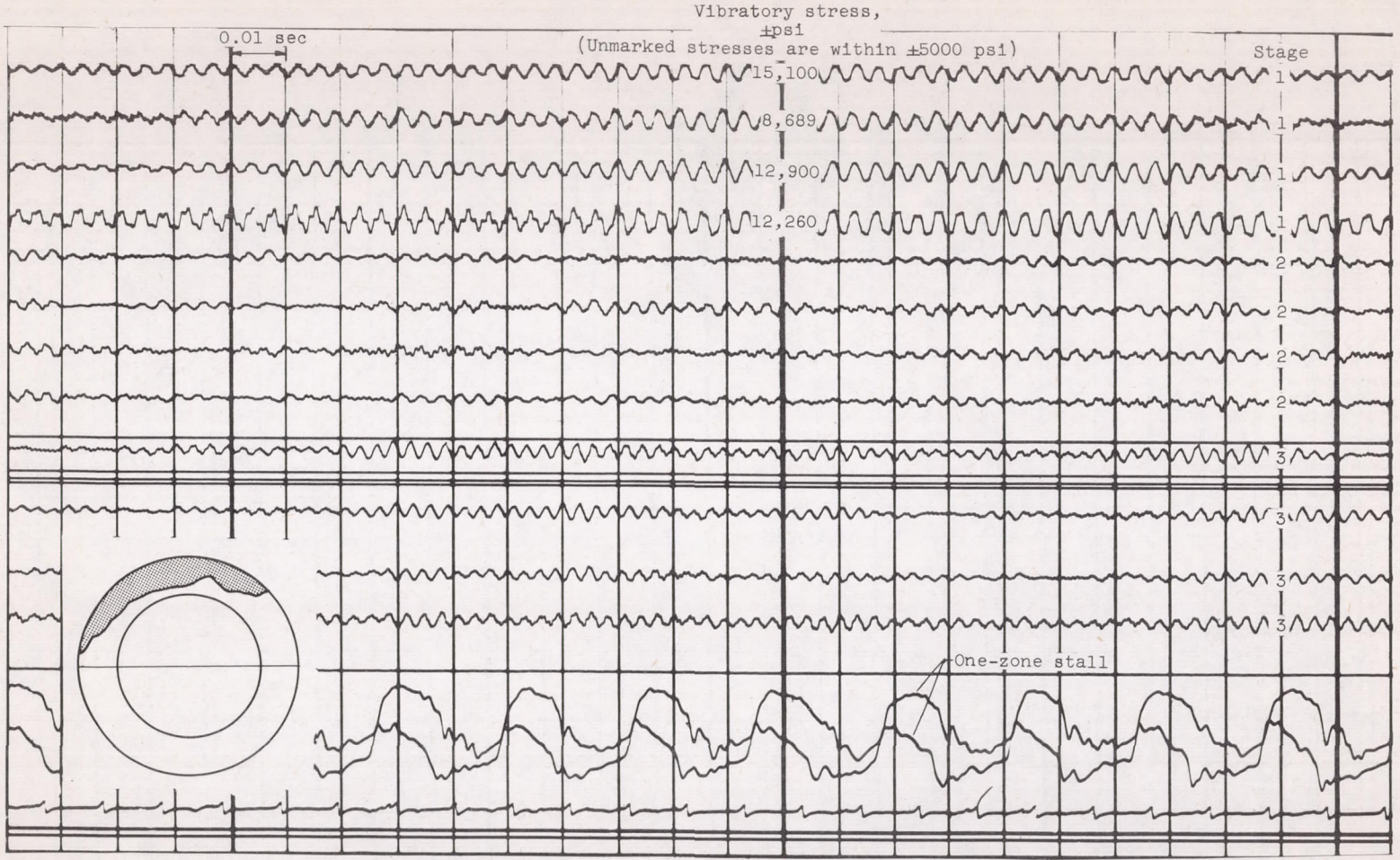

(c) Section c of figure 8. Actual engine speed, 5700 rpm.

Figure 12. - Concluded. Oscillogram showing effect of changing the number of zones per stall pattern from three to one on first- and second-stage blade vibration.

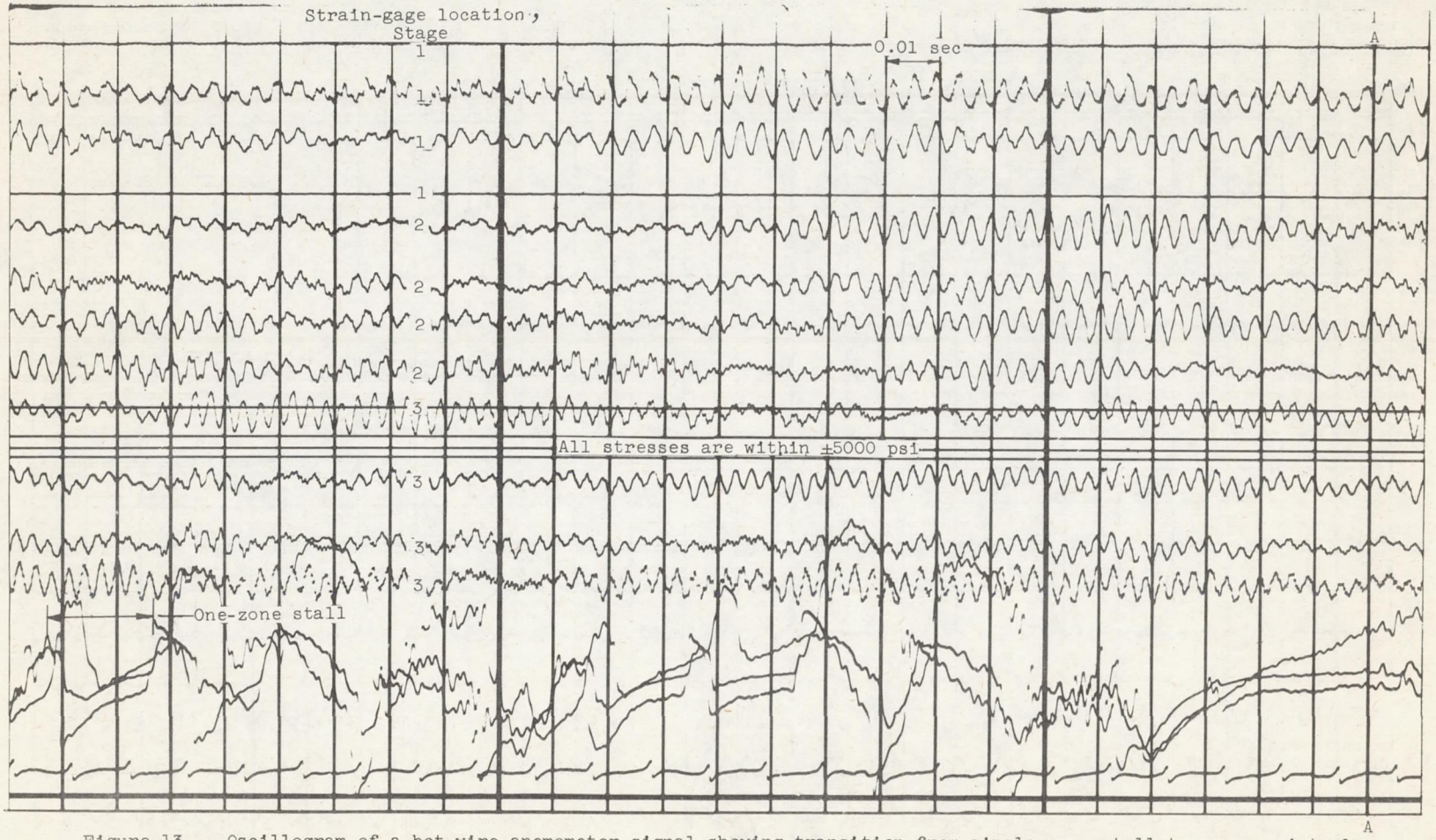

Figure 13. - Oscillogram of a hot-wire anemometer signal showing transition from single-zone stall to surge. Actual engine speed, 5786 rpm.

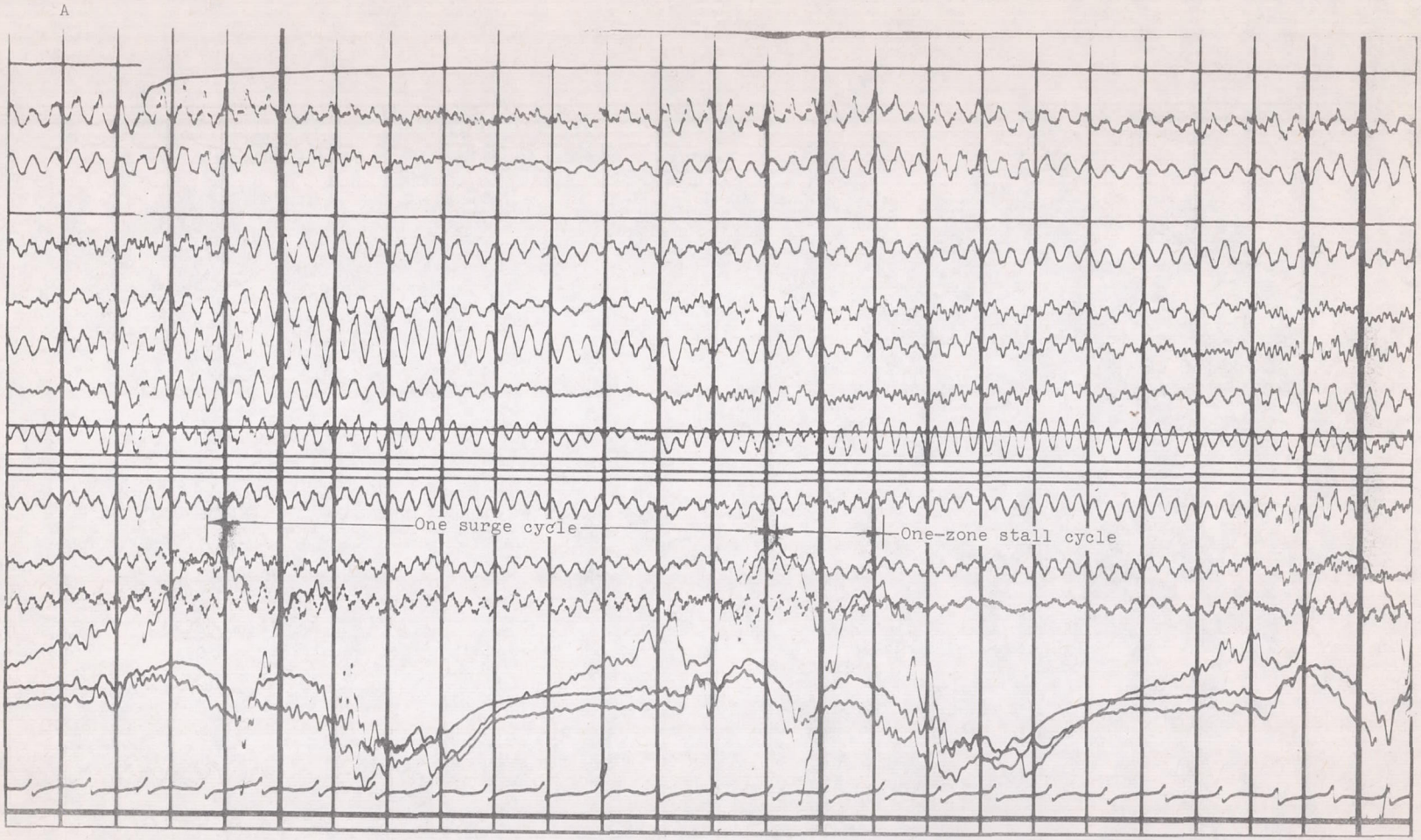

Figure 13. - Concluded. Oscillogram of a hot-wire anemometer signal showing transition from single-zone stall to surge. Actual engine speed, 5786 rpm.